# CANADIAN JOURNAL OF RESEARCH

VOLUME 25 NOVEMBER, 1947 NUMBER 6


— SECTION A —

## PHYSICAL SCIENCES

### *Contents*


| | Page |
|---|---|
| The Absorption of Gamma-rays from $Co^{60}$—*W. V. Mayneord and A. J. Cipriani* | 303 |
| The *E*-plane Radiation Pattern of Short Electromagnetic Horns of Large Aperture—*G. A. Woonton and J. G. Tillotson* | 315 |
| The Use of Diaphragms in the Electron Microscope—*S. G. Ellis* | 322 |
| A Low-pressure Glow-discharge Proton Source—*Paul Lorrain* | 338 |
| Thermal Conductivity of Metals at High Temperatures. I. Description of the Apparatus and Measurements on Iron—*L. D. Armstrong and T. M. Dauphinee* | 357 |



NATIONAL RESEARCH COUNCIL
OTTAWA, CANADA

## CANADIAN JOURNAL OF RESEARCH

The *Canadian Journal of Research* is issued in six sections, as follows:

| | |
|---|---|
| A. Physical Sciences | D. Zoological Sciences |
| B. Chemical Sciences | E. Medical Sciences |
| C. Botanical Sciences | F. Technology |

For the present, each of these sections is to be issued six times annually, under separate cover, with separate pagination.

The *Canadian Journal of Research* is published by the National Research Council of Canada under authority of the Chairman of the Committee of the Privy Council on Scientific and Industrial Research. The *Canadian Journal of Research* is edited by a joint Editorial Board consisting of members of the National Research Council of Canada, the Royal Society of Canada, and the Chemical Institute of Canada.

Sections B and F of the *Canadian Journal of Research* have been chosen by the Chemical Institute of Canada as its medium of publication for scientific papers.



### EDITORIAL BOARD

| *Representing* National Research Council | *Representing* Royal Society of Canada | |
|---|---|---|
| Dr. J. B. Collip *(Chairman)*, Director, Research Institute of Endocrinology, McGill University, Montreal. | Dr. A. Norman Shaw, Chairman, Department of Physics, McGill University, Montreal. | Section III |
| Dr. Paul E. Gagnon, Director of the Graduate School, Laval University, Quebec. | Dr. J. W. T. Spinks, Department of Chemistry, University of Saskatchewan, Saskatoon. | |
| Dr. A. R. Gordon, Head, Department of Chemistry, University of Toronto, Toronto. | Professor J. R. Dymond, Director, Royal Ontario Museum of Zoology, Toronto. | Section V |
| Dr. J. A. Gray, Professor of Physics, Queen's University, Kingston. | Dr. H. S. Jackson, Head, Department of Botany, University of Toronto, Toronto. | |

| *Ex officio* | *Representing* The Chemical Institute of Canada |
|---|---|
| Dr. Léo Marion, Editor-in-Chief, Department of Chemistry, National Research Laboratories, Ottawa. | Dr. R. V. V. Nicholls, Associate Professor of Chemistry, McGill University, Montreal. |

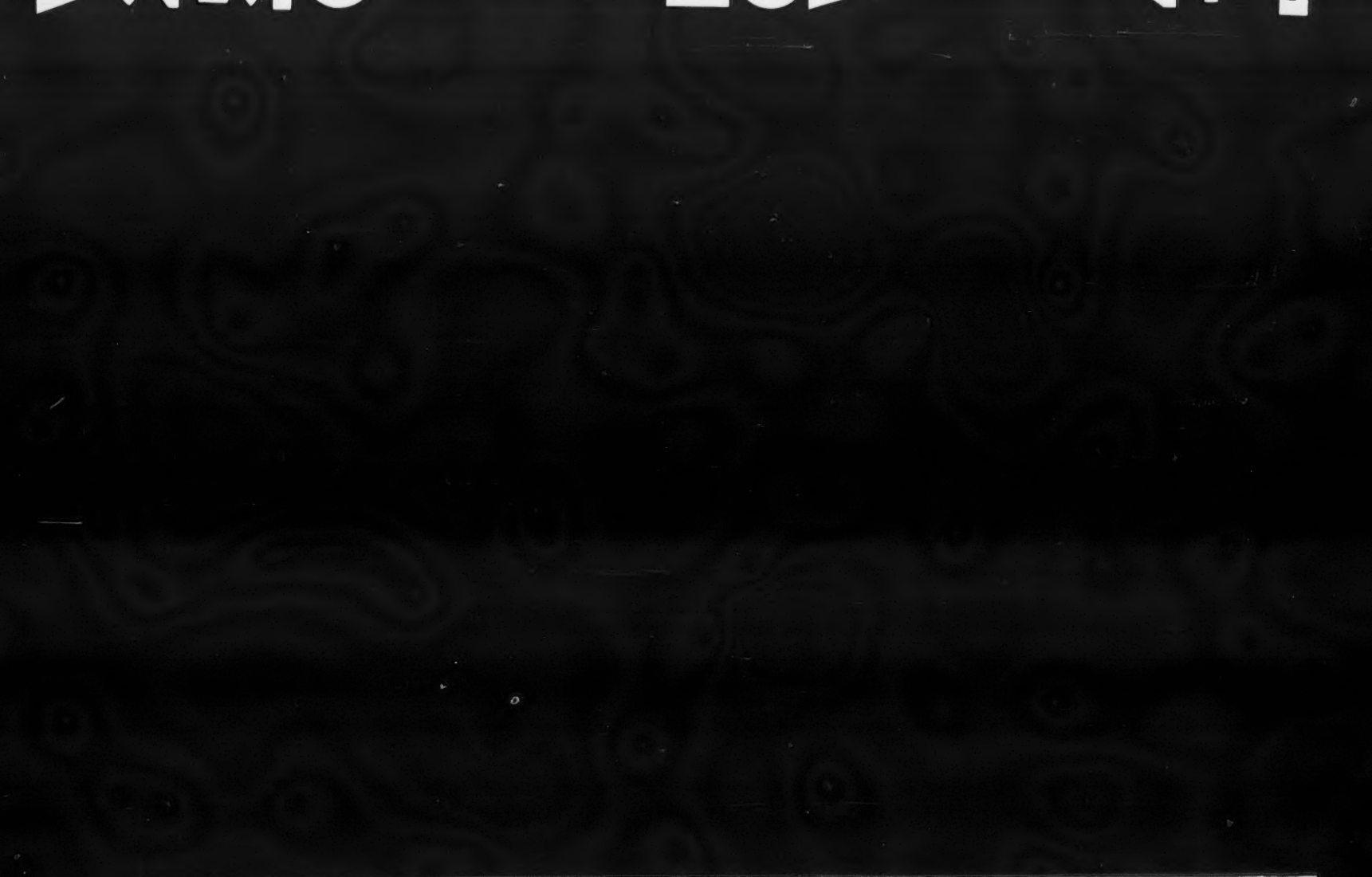
### Editorial Committee

| | |
|---|---|
| Editor-in-Chief, | Dr. Léo Marion |
| Editor, Section A, | Dr. A. Norman Shaw |
| Editor, Section B, | Dr. J. W. T. Spinks<br>Dr. R. V. V. Nicholls |
| Editor, Section C, | Dr. H. S. Jackson |
| Editor, Section D, | Professor J. R. Dymond |
| Editor, Section E, | Dr. J. B. Collip |
| Editor, Section F, | Dr. J. A. Anderson<br>Dr. R. V. V. Nicholls<br>Dr. A. Norman Shaw |



Manuscripts should be addressed:

*Editor-in-Chief,*
*Canadian Journal of Research,*
*National Research Council, Ottawa, Canada.*



# Canadian Journal of Research

*Issued by* THE NATIONAL RESEARCH COUNCIL OF CANADA

VOL. 25, SEC. A. NOVEMBER, 1947 NUMBER 6


## THE ABSORPTION OF GAMMA-RAYS FROM $Co^{60}$ [1]


BY W. V. MAYNEORD[2] AND A. J. CIPRIANI[3]



### Abstract

Measurements of the absorption of gamma-rays from $Co^{60}$ and radium have been made in a number of materials. Variation of absorption coefficient of the gamma-rays from radium with thickness of lead absorber is in agreement with recent experimental determinations. The gamma-rays from $Co^{60}$ are approximately monochromatic and are therefore suitable for testing theoretical absorption formulae. The absorption coefficient per electron for materials of atomic number equal to or less than that of aluminium was in agreement with the Klein–Nishina formula, assuming the cobalt radiation to consist of two lines at 1.10 and 1.30 Mev. respectively. The photoelectric absorption coefficients per electron for heavy elements are in good agreement with the theory developed by Hulme, McDougall, Buckingham, and Fowler. This coefficient varies approximately as $Z^{3.5}$.


### Introduction

Among the artificial radioactive substances $Co^{60}$, owing to its relatively long life, is a convenient laboratory gamma-ray standard and a possible substitute for radium in certain therapeutic applications. It was therefore thought of importance to determine the absorption coefficients of its radiations in a number of materials, particularly as the approximate homogeneity of these radiations affords an opportunity to test theoretical formulae for absorption coefficients much more accurately and conveniently than by the use of the complex radiations from radium preparations.

Preliminary experiments were, however, carried out with Ra (B + C) sources as a check on the experimental arrangements adopted.

### Sources of Radiation

The Ra (B + C) source consisted of a Monel cylinder 6.3 mm. diameter and approximately 7.0 mm. long containing 100 mgm. radium element, the whole constituting a standard industrial radiographic source. The active material was enclosed in a cylindrical volume 4 mm. long and 4 mm. diameter, the wall being approximately 1 mm. Monel.


[1] *Manuscript received May 9, 1947.*

*Contribution from the Biological and Medical Research Branch of the Atomic Energy Project, National Research Council of Canada, Chalk River, Ont. Issued as N.R.C. No. 1610.*



[2] *Physicist, Royal Cancer Hospital, London, England. Adviser to the Biological and Medical Research Branch of the Atomic Energy Project, Chalk River, Ont., 1945-1946.*

[3] *Chairman, Biological and Medical Research Branch of the Atomic Energy Project, Chalk River, Ont.*

The beam of gamma-rays was canalized by placing the source at one end of a tapered hole in a lead block as shown in Fig. 1. This tapered hole was cast in a simple cylinder of lead that fitted inside a larger cylinder of lead of

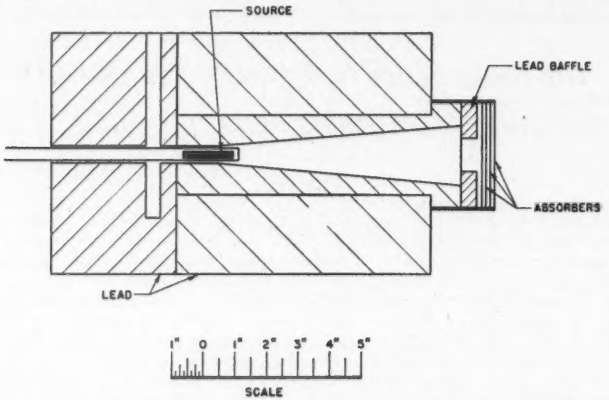



FIG. 1. *Longitudinal section through collimating block used in absorption measurements.*

the dimensions indicated; a third cylinder of lead was placed behind the collimator for shielding purposes. For convenience in handling, the 100 mgm. source was held in the end of a brass rod turned and sprung to grip it tightly. The cylindrical protective lead block rested on two strips of angle iron, welded to a steel plate. Duralumin tubes, slipped into the angle iron, served as convenient handles and also as adjustable supports for a small wooden table on which absorbers could be supported. Lead baffles having various apertures were machined and placed in the mouth of the taper so as to absorb secondary radiation from the inside of the tapered hole, but these baffles were found to have little effect on the observed absorption coefficients. The distance from centre of radium source to centre of ionization chamber was approximately 72 cm. and the distance between the aperture of the tapered hole and chamber, 51 cm. In these circumstances the scattered radiation from the absorber reaching the chamber was not greater than 2% of the total scatter, but, when necessary, appropriate corrections have been made.

The cobalt source consisted of about 20 gm. of metallic cobalt of total gamma-ray activity equivalent to that of 255 mgm. radium. This material was packed as tightly as possible into a brass cylinder of wall thickness 0.8 mm., which was then soldered. The active volume measured 5.5 cm. long and 1.0 cm. diameter. When placed in the tapered hole so as to give the optimum canalization, the position was as shown in Fig. 1. Most of the measurements were thus made with the radiation emerging from the end of the source, but some observations are also made of the radiation emerging at right angles as also indicated in Fig. 1, thus largely avoiding the absorption loss in the material itself.

## Measuring System

The measuring system, originally designed for gamma-ray dosimetry, usually consisted of a small cylindrical ionization chamber, 2.540 cm. internal diameter and 2.540 cm. internal length, on the end of a long lead evacuated with a rotary oil pump to avoid stray ionization in the system. The apparatus, Fig. 2, was so designed that chambers of any size, shape, or material could readily be screwed into position, the outside of the chamber being raised to the necessary saturation potential. The insulated central lead of the chamber

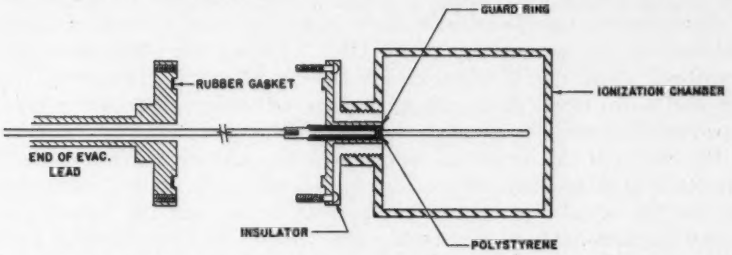



FIG. 2. *Mid-section through ionization chamber and end of evacuated lead.*

was connected to the grid of an FP-54 tube in a slightly modified DuBridge-Brown balanced circuit (2), the deflection of the galvanometer being a measure of the ionization current in the chamber. In preliminary experiments the balance of the circuit and its characteristics were investigated and found satisfactory. After the tube had been aged by continuous running for a fortnight, the stability of zero was satisfactory over times of the order of a few hours. The galvanometer deflection increased linearly with grid potential change (as determined with a Leeds Northrup type K potentiometer) over the whole galvanometer range (maximum current approximately 0.3 $\mu$a.) to within 1%. Consequently, the quicker direct deflection method was usually employed during absorption measurements in place of potentiometer compensation. A Victoreen grid leak of the order of $10^{11}$ ohms was used in most experiments but $10^{12}$ ohms was also available if higher sensitivity was required. Both FP-54 and grid leak were enclosed in a heavy brass chamber, which was evacuated with the ionization chamber lead. The high speed of response with the $10^{11}$ ohms grid leak (full deflection in approximately 10 sec.) and the slow nature of the zero drifts made the operation of measuring radiation absorption very quick, so that in a few minutes the whole absorption curve of a given substance could be investigated, and frequent repetition experiments were possible. In general, the repetition of percentage transmissions is better than 1% and the final absorption coefficients are estimated to be accurate to approximately $\pm$ 1%.

Most of the absorption coefficients have been determined using an aluminium ionization chamber of the internal dimensions indicated and 3 mm. wall thickness to avoid so far as possible the complex variation of ionization

function due to photoelectric effect in the chamber wall and to build up the appropriate electronic equilibrium. For a monochromatic radiation the observed absorption coefficient should be independent of chamber material, and we have found for $Co^{60}$ radiation good agreement between absorption coefficients in light elements as measured in chambers of carbon, aluminium, and even lead. Small differences are observed during measurements of absorption in heavy elements with a lead chamber (Fig. 5).

## The Absorption of Gamma-rays from Ra (B + C)

Measurements have been made of the absorption coefficients in aluminium and lead for the gamma-rays of Ra (B + C) using the canalized beam as described. A number of experimenters have investigated this subject (7, pp. 466-480) and it is well known that the observed coefficients depend upon the experimental conditions adopted, the main difficulties lying in the assessment of the effects of the ionization functions of the ionization chambers, initial uncertainties in the energy distribution in the complex Ra (B + C) gamma-ray spectra, the initial filtrations of the primary beam, and the magnitude of scatter corrections depending on the geometry of the experimental set-up. The radium source is, in fact, fundamentally unsuited to any attempt to test theoretical formulae for variation of absorption coefficient with atomic number and quantum energy.

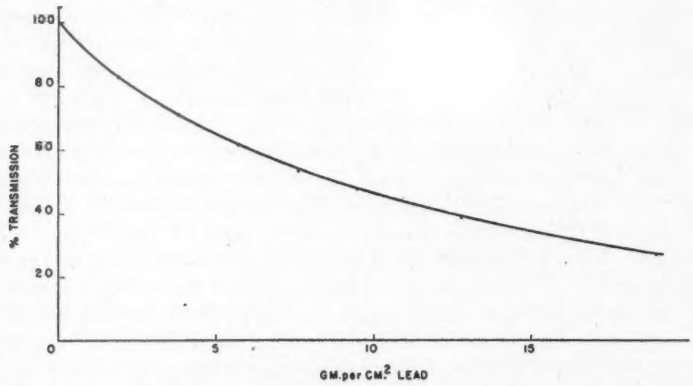



FIG. 3. *Transmission curve in lead for gamma-rays from* Ra (B + C) *obtained with an aluminium ionization chamber.*

The lead absorbers employed were machined lead disks approximately 1.68 mm. thick and 7.620 ± 0.005 cm. diameter, each of which was weighed. The mean transmission curve as measured in an aluminium chamber is shown in Fig. 3. The logarithmic transmission curve is not straight so that the definition of absorption coefficient at a given filtration becomes of importance. The absorption coefficient should be defined by the tangent to the logarithmic

transmission curve at the filtration of interest, but in view of the uncertainties of drawing such curves the values adopted are those obtained by considering the decrease of transmission caused by three of the experimental filters, namely, a total of 5.76 gm. per cm.$^2$ of lead. The initial filtration due to 1/16 in. copper sheet placed over the aperture of the beam to remove secondary electrons and soft radiation and the 1 mm. of Monel in the wall of the source itself was regarded as equivalent to 2.0 mm. lead (2.3 gm. per cm.$^2$).

The variation of absorption coefficient with thickness of lead absorber is shown in Fig. 4. The absorption coefficients agree at high filtrations with the

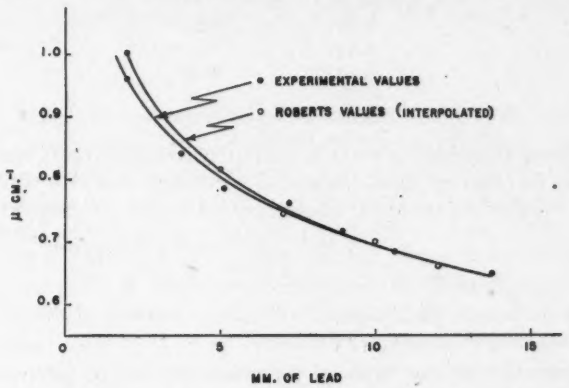



FIG. 4. *Variation of linear absorption coefficient with thickness of lead filter for gamma-rays from* Ra (B + C).

recent careful measurements by Roberts (6), but are lower at low filtrations, possibly owing to the thickness of standard absorber chosen. In agreement with Roberts we find absorption coefficients below those given by Rutherford, Chadwick, and Ellis, probably owing to the choice of a low atomic number for the ionization chamber. It is, however, interesting to note that if the absorption coefficients measured by us were regarded as corresponding to a filtration equal to the initial filtration plus 2.5 mm. of lead (half the thickness of the test absorber) then our experimental results agree fairly well with the Rutherford, Chadwick, and Ellis curve.

It is clear that great care is required in the definition and measurement of the absorption coefficient of a beam containing such varied quanta as those emitted by Ra (B + C).

## Experimental Results for the Gamma-rays of $Co^{60}$

The absorption coefficients of a number of substances have been measured for the gamma-rays of $Co^{60}$ using an aluminium chamber and radioactive source end-on as already described. The results of these measurements are given below. All absorbers with the exception of mercury were carefully

weighed and their mass absorption coefficients determined directly, electronic and linear absorption coefficients being subsequently deduced. The linear absorption coefficient of liquid mercury was measured directly as described below.

*Beryllium*

Metallic beryllium was available in large, approximately rectangular blocks of assorted sizes which could be combined to make suitable absorbers. The mean percentage transmissions through varying thickness are given below.

| Absorber, gm. per cm.$^2$ | % Transmission |
|---|---|
| 0.00 | 100.0 |
| 5.80 | 75.1 |
| 11.85 | 55.0 |
| 17.58 | 41.4 |
| 23.42 | 30.9 |

The logarithmic transmission curve is accurately straight to 30% transmission, and leads to an observed mass absorption coefficient $\mu/\rho = 0.0505$ cm.$^2$ per gm. The uncorrected electronic absorption coefficient is therefore:

$$\mu_\epsilon = 1.89 \times 10^{-25} \text{ cm.}^2 \text{ per electron,}$$

$$\text{since } \mu_\epsilon = \mu/\rho \times A/Z \times 6.02 \times 10^{23},$$

where $A$ is the atomic weight and $Z$ the atomic number of the element considered, $\rho$ the density in gm. per cm.$^3$

Measurements were also made of the absorption of the gamma-rays from radium in beryllium using two 100 mgm. Monel enclosed sources in tandem.

The corrected absorption coefficients were $\mu/\rho = 0.0535$ or $\mu_\epsilon = 2.01 \times 10^{-25}$ cm.$^2$ per electron.

With a filter of 12 mm. lead the mass absorption coefficient was 0.0445 or $\mu_\epsilon = 1.67 \times 10^{-25}$ cm.$^2$ per electron.

*Carbon*

The absorption was measured in accurately cylindrical blocks of pure graphite machined to $3.000 \pm 0.002$ in. diameter and of various thicknesses. All filters were weighed. The mean logarithmic transmission curve shows no deviation from a straight line to 25 gm. per cm.$^2$ and leads to uncorrected absorption coefficients,

$$\mu/\rho = 0.0549 \text{ cm.}^2 \text{ per gm. and } \mu_\epsilon = 1.83 \times 10^{-25} \text{ cm.}^2 \text{ per electron.}$$

In the experiments on beryllium and carbon the thickness of absorber required was such as to bring the scattering material appreciably nearer the ionization chamber than the exit of the taper hole, and it became necessary to consider scatter corrections to the observed absorption coefficients.

The theory of such scattering corrections has been studied by a number of workers, both Tarrant (9) and Tandberg (8) having given formulae for the corrections involved. Under the conditions here considered the correction is

small and may be made using Tarrant's formula for the difference between the true and apparent electronic coefficients, namely:

$$\mu_e \text{ true} - \mu_e \text{ app.} = \frac{\pi e^4}{m^2c^4} \cdot \theta^2 \left\{ 1 + \frac{\theta^2}{4}(5.5\,\alpha - 1) \right\},$$

where $\theta$ is the maximum angle of scatter into the chamber, $\alpha = h\nu/mc^2$.

For the cobalt radiation $\alpha = 2.4$ and the maximum angle of scatter in the carbon experiments 0.13 radians, so that the maximum scatter correction is $0.04 \times 10^{-25}$. Taking into account the appropriate geometry for each element, the corrected values of the electronic absorption coefficients for beryllium and carbon respectively are $1.92 \times 10^{-25}$ and $1.87 \times 10^{-25}$ cm.$^2$ per electron.

*Water*

From a biological and medical point of view the absorption in water is clearly of great importance and observations were, therefore, made of the absorption coefficient in water. Several lucite cells were constructed, a typical example having a watertight lid held in position by 12 screws and containing a cylinder of liquid 3.000 in. diameter and 1.000 in. long. The dimensions were verified by weighing, the mass of water per square centimetre in this instance being found to be 2.54 gm. per cm.$^2$ In preliminary experiments on the empty cells the absorption in the ends, 1.00 mm. thick, was found and allowance made in the final results. The mean of a number of experiments gave the percentage transmission of the $Co^{60}$ gamma-rays through 2.54 gm. per cm.$^2$ of water as 85.2%, with corresponding coefficients $\mu/\rho =$ 0.0632 cm.$^2$ per gm. or $\mu_e = 1.90 \times 10^{-25}$ cm.$^2$ per electron.

It was also thought of interest to measure the absorption coefficients in heavy water, since the experiment affords an opportunity to investigate the abnormally high mass absorption coefficient of hydrogen compared to that of other light elements. On substituting deuterium for normal hydrogen, the number of electrons per molecule remains constant but the mass is, of course, increased.

The lucite cell was carefully filled with heavy water (99.7% purity), and the transmission again measured. The observed percentage transmission through the cell was now 85.3%, in good agreement with the result for normal water and demonstrating that the linear absorption coefficients in water and heavy water are identical. The mass of heavy water filling the cell was 128.13 gm. as compared to 115.78 gm. of water, the relative densities being therefore 1.107. The measured absorption coefficients for water and heavy water were as follows:

| Water | Heavy water |
|---|---|
| $\mu/\rho = 0.0632$ cm.$^2$ per gm. | $\mu/\rho = 0.0568$ cm.$^2$ per gm. |
| $\mu_e = 1.90 \times 10^{-25}$ cm.$^2$ per electron | $\mu_e = 1.89 \times 10^{-25}$ cm.$^2$ per electron |
| $\mu = 0.0632$ cm.$^{-1}$ | $\mu = 0.0630$ cm.$^{-1}$ |

It is interesting to note that for gamma-ray absorption deuterium is the 'normal' element and 'ordinary' hydrogen the abnormal material. (See Table I.) These conclusions are in agreement with experiments carried out some years ago (5) by one of us using X-rays produced at 400 kv.

*Aluminium*

The absorption of $Co^{60}$ gamma-rays was measured in carefully machined disks of pure aluminium of varying thicknesses and diameter $3.000 \pm 0.002$ in. The straight logarithmic absorption curve gave $\mu/\rho = 0.0550$ cm.$^2$ per gm. and $\mu/\epsilon = 1.90 \times 10^{-25}$ cm.$^2$ per electron.

A lead ionization chamber was also used for the absorption measurements. The results were the same, within experimental error, as those obtained with an aluminium ionization chamber. This would, of course, be expected for a homogeneous radiation and a light element. It was later shown that the apparent absorption coefficient in lead is different when measured in lead and aluminium chambers, even for $Co^{60}$ radiations.

*Heavy Elements*

Measurements have also been made with a number of heavier elements in order to investigate the photoelectric absorption coefficients. The method of measurement was as previously described and calls for no further comment.

The elements investigated were in the form of accurately machined circular disks and included mild steel, pure electrolytic copper, fine silver, platinum, lead, bismuth, and uranium. The absorption in metallic mercury was found

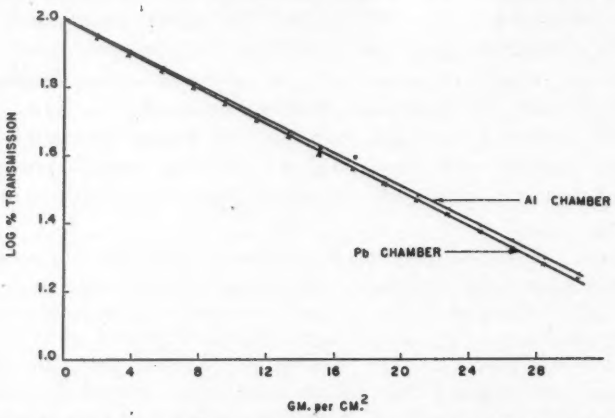



FIG. 5. *Logarithmic transmission curve in lead for gamma-rays from* $Co^{60}$ *obtained with an aluminium ionization chamber and a lead chamber.*

by filling a glass cell whose absorption when empty was known, and inserting lucite blocks of known absorbing properties so as to give varying thicknesses of mercury, care being taken to ensure complete displacement of the

liquid. By measuring the dimensions of the glass cell and lucite blocks the thickness of the mercury layer could be found and hence the linear absorption coefficient.

A number of measurements have also been made with metallic uranium which was available in the form of disks of thickness approximately 7 gm. per cm.$^2$ This material is of particular interest as it affords the opportunity to test the variation of photoelectric coefficient with atomic number for the highest atomic numbers, in which region experimental results have hitherto been uncertain. From a practical point of view the high density and high absorption per electron combine to give metallic uranium a high linear absorption coefficient, which makes it a particularly valuable shielding material with considerable application in medicine and experimental work generally. Fig. 5 shows the logarithmic absorption curves in lead as measured with aluminium and lead chambers respectively. The absorption curve in lead of radiation emitted at right angles to the axis of the cobalt source and measured in an aluminium chamber is indistinguishable from the mean of these two curves.

## Experimental Results and Discussion

We give below (Table I) the experimental absorption coefficients, corrected where necessary for scatter, while Fig. 6 shows a few examples of the logarithmic transmission curves from which the coefficients were derived. No evidence of high energy ( $> 1.5$ Mev.) components in the $Co^{60}$ gamma-ray spectrum was obtained, but such components, if weak, might still be revealed by a study of transmissions at larger thickness of absorber than that used by us.

TABLE I

| Material | Atomic No., $Z$ | Atomic wt., $A$ | Experimental $\mu/\rho$, cm.$^2$ per gm. | Corrected $\mu_a$, cm.$^2$ per electron $\times 10^{25}$ | $\tau_a$ |
|---|---|---|---|---|---|
| Be | 4 | 9.02 | 0.0505 | 1.92 | 0.00 |
| C | 6 | 12.01 | 0.0549 | 1.87 | 0.00 |
| $H_2O$ | '5' | '9.008' | 0.0632 | 1.90 | 0.00 |
| $D_2O$ | '5' | '10.015' | 0.0568 | 1.89 | 0.00 |
| Al | 13 | 26.97 | 0.0550 | 1.90 | 0.00 |
| Steel | 26 | 55.85 | 0.0538 | 1.92 | 0.02 |
| Cu | 29 | 63.57 | 0.0531 | 1.94 | 0.04 |
| Ag | 47 | 107.88 | 0.0519 | 1.98 | 0.08 |
| Pt | 78 | 195.32 | 0.0576 | 2.41 | 0.51 |
| Hg | 80 | 200.61 | 0.0578 | 2.41 | 0.51 |
| Pb | 82 | 207.21 | 0.0573 | 2.42 | 0.52 |
| Bi | 83 | 209.00 | 0.0588 | 2.47 | 0.57 |
| U | 92 | 238.07 | 0.0638 | 2.74 | 0.84 |

The values given in Table I are for absorber thicknesses up to 10 gm. per cm.$^2$ For heavy elements (e.g., lead and bismuth) there is some evidence that the logarithmic transmission curve departs from linearity at greater thicknesses by an amount in agreement with the theory discussed below.

It will be seen that elements of low atomic number for which photoelectric absorption is negligible yield a constant value of electronic coefficient whose mean value is $1.90 \times 10^{-25}$ cm.$^2$ per electron. The absorption coefficient

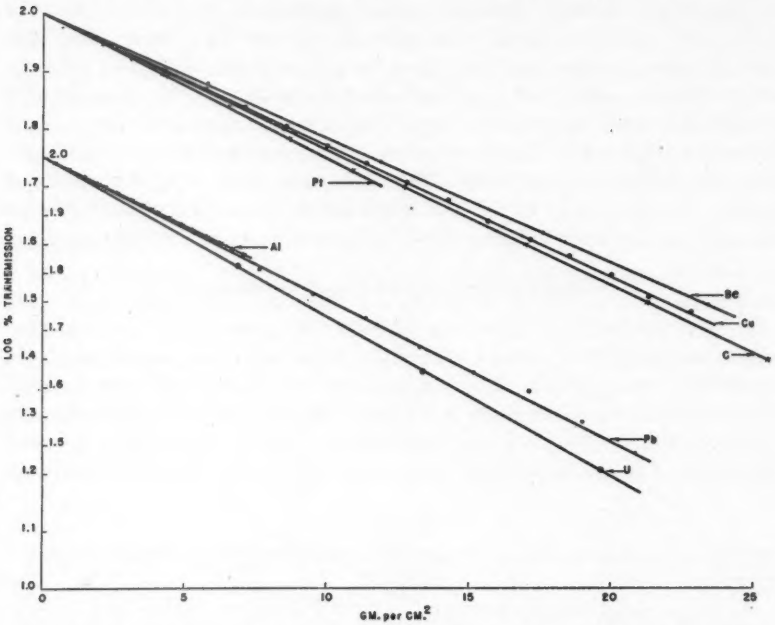



FIG. 6. *Logarithmic transmission curve in some of the elements studied for the gamma-rays from* $Co^{60}$.

would correspond, according to the Klein–Nishina formula (4), to a value of $h\nu/mc^2$ equal to 2.40 or an average quantum energy of 1.22 Mev. As the result of beta-ray studies, Deutsch, Elliott, and Roberts (1) gave the energies of the $Co^{60}$ lines as $1.10 \pm 0.03$ and $1.30 \pm 0.03$ Mev., respectively, which would correspond to a mean energy of 1.21 Mev. Our absorption measurements are, therefore, in good agreement with the beta-ray results and lie within the experimental error of those experiments. Alternatively, the agreement may be regarded as verifying the Klein–Nishina calculations of scattering absorption coefficients. Comparison may also be made with the theory of photoelectric absorption given by Hulme, McDougall, Buckingham, and Fowler who give their results (3) in the form of a graph of a calculated function

of the photoelectric absorption coefficient per atom over a range of atomic number and quantum energies. Values of photoelectric absorption coefficients per electron, deduced by graphical interpolation from their results for the elements measured by us, are given in the Table II below for $\alpha = 2.40$.

The experimental values of $\tau_\epsilon$ are obtained by subtracting $1.90 \times 10^{-25}$ from the measured total absorption coefficient per electron, pair formation being negligible for $Co^{60}$ radiation.

The Hulme theory does not lead to any simple relation between $\tau_\epsilon$ and $Z$, but suggests a variation of $\tau_\epsilon$ roughly proportional to $Z^{3.56}$, which is distinctly faster than $Z^3$, over the region of $Z$ from 10 to 80 for the radiation having $\alpha = 2.40$. The theoretical and experimental values of $\mu$ per electron are plotted against $Z$ in Fig. 7 and the values of $\tau_\epsilon$ given in Table II.

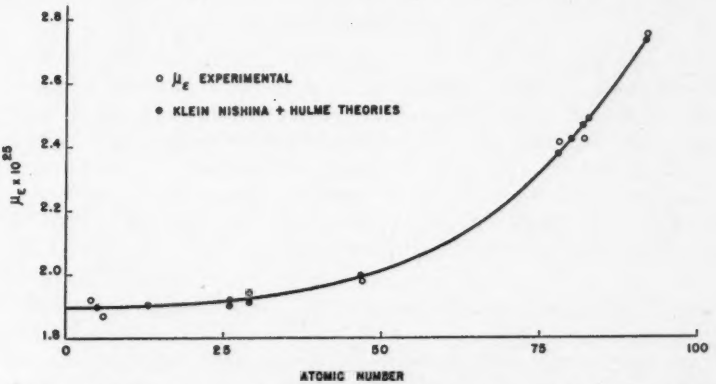



FIG. 7. *Theoretical and experimental values of the absorption coefficient per electron plotted against atomic number Z.*

TABLE II

| $Z$ | $\tau_\epsilon \times 10^{25}$ | | $Z$ | $\tau_\epsilon \times 10^{25}$ | |
|---|---|---|---|---|---|
| | Theoretical | Experimental | | Theoretical | Experimental |
| 26 | 0.01 | 0.02 | 80 | 0.51 | 0.51 |
| 29 | 0.02 | 0.04 | 82 | 0.56 | 0.52 |
| 47 | 0.09 | 0.08 | 83 | 0.57 | 0.57 |
| 78 | 0.47 | 0.51 | 92 | 0.83 | 0.84 |

It will be seen that the experimental and theoretical results for $\tau_\epsilon$ are also in good agreement. We conclude, therefore, that both scattering and photoelectric theories are satisfactory in the region of 1.2 Mev. It would be of considerable interest to repeat the experiments with a substantially monochromatic radiation in a different energy region.

## References

1. DEUTSCH, M., ELLIOTT, L. G., and ROBERTS, A. Phys. Rev. 68 : 193-197. 1945.
2. DUBRIDGE, L. A. and BROWN, H. Rev. Sci. Instruments, 4 : 532-536. 1933.
3. HULME, H. R., MCDOUGALL, J., BUCKINGHAM, R. A., and FOWLER, R. H. Proc. Roy. Soc., London, A149 : 131-151. 1935.
4. KLEIN, O. and NISHINA, Y. Z. Physik, 52 : 853-868. 1929.
5. MAYNEORD, W. V. and ROBERTS, J. E. Nature, 136 : 793. 1935.
6. ROBERTS, J. E. Proc. Roy. Soc., London, A183 : 338-355. 1945.
7. RUTHERFORD, E., CHADWICK, J., and ELLIS, C. D. Radiations from radioactive substances. Cambridge Univ. Press, London. 1930.
8. TANDBERG, J. Inaugural Dissertation, University of Uppsala. 1937.
9. TARRANT, G. T. P. Proc. Cambridge Phil. Soc. 28 : 475-489. 1932.

# THE *E*-PLANE RADIATION PATTERN OF SHORT ELECTROMAGNETIC HORNS OF LARGE APERTURE[1]

By G. A. Woonton[2] and J. G. Tillotson[3]


## Abstract

The relation between the power received by a short, rectangular, electromagnetic horn, and its angular position in a plane electromagnetic field can be calculated, for rotation in the plane of the electric vector, from ordinary optical theory by assuming that the aperture produces at the throat a Fresnel diffraction pattern appropriate to the angular position of the aperture. Experimental results for four horns of slant lengths 25, 50, 100, and 176 cm., but all of the same aperture, $10\lambda$ to a side at a wave length of 3.2 cm., are in good agreement with the theoretical predictions at angles up to $\frac{1}{4}$ radian from the axis, for slant lengths down to 50 cm. but not down to 25 cm.


## Introduction

The diffraction pattern of an aperture as discussed in physical optics and the radiation pattern of an antenna both result from the same physical phenomena; the close relation between the two is particularly apparent if the antenna is a microwave electromagnetic horn. In that case the electromagnetic wave which falls on the mouth of the horn and converges on the throat, or which diverges from the throat to be radiated from the mouth, can be identified with a light wave that falls on a slit in a screen, to be diffracted to a field point, or which diverges from a point source to fall on a slit and form a diffraction pattern.

Mathematical relations which are adequate for the prediction of optical diffraction patterns must be used with caution when applied to the prediction of microwave radiators. This is not due to any difference in phenomena; the discrepancies appear because of the very great difference in the relative dimensions of the waves and the apparatus in the two cases. The approximations which are inherent in the optical, Huygens–Kirchhoff method of calculation are of two kinds: fundamental approximations which are essentially a misstatement of the nature of the phenomena, and superficial approximations of trigonometry and algebra, which are introduced to simplify mathematical manipulations. Errors due to the first kind of approximation are most serious when the dimensions of the aperture are comparable with the wave length; errors due to trigonometrical and algebraic approximations become important when the point at which the field is to be predicted is taken at a relatively few wave lengths from the aperture.

The radiation patterns of apertures of various shapes have been predicted by Barrow and collaborators, by Chu, and by Schelkunoff (1; 2; 3; 4, Chap. IX), by methods which are exact in the statement of boundary conditions,

[1] *Manuscript received June 20, 1947.*
*Contribution from the Department of Physics, University of Western Ontario, London, Ont.*
[2] *Research Professor.*
[3] *Demonstrator.*

but which, like the method of Kirchhoff, contain approximations which lead to progressive error as the field point approaches the aperture. We have not been able to evaluate as yet the near field error in these methods, nor have we been able to predict the errors in the Kirchhoff method by any analytical means which will yield information on the error as a function of the distance from field point to aperture. Although an analytical check of the errors in the various formulae has not been possible, the accuracy of the formulae for the prediction of the near field of an aperture can be tested by using them to predict the power at the throat of a horn antenna as it is rotated in an electromagnetic field. This paper reports a comparison between the measured values of power for a set of electromagnetic horns operated at a wave length of 3.2 cm. and values predicted by optical theory involving the Fresnel integrals.

## Method and Apparatus

The term 'radiation pattern' as applied to microwave antennae usually means a graph of the relative power supplied by the antenna to some detecting device, plotted against the angular position of the antenna when it is rotated in a uniform, plane-polarized electromagnetic field. The relative power at the throat of an electromagnetic horn was calculated by the use of the Fresnel integrals applied to the mouth of the horn as if it were a slit undergoing rotation in a uniform field, and these data have been plotted as the predicted radiation patterns in Figs. 2, 3, 4, and 5. The details of the mathematical method are sketched in Fig. 1; the plane of this figure is the *E*-plane or plane of the electric vector of the polarized radiation from the source *S*. The horn is rotated about a point *C*, on its axis of symmetry at a distance *a*, the slant

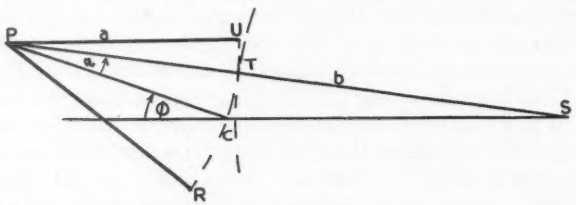



FIG. 1. *Plan view of source, turntable, and horn.*

*The plane of this figure is the plane of the electric vector of the polarized radiation from the source S.*

*S — Source of 3.2 cm. radiation.*
*P — Vertex of the electromagnetic horn UPR.*
*C — Centre of rotation for the horn.*
*T — Pole of the wave proceeding from S to P.*
$\phi$ — *Angular displacement of the horn axis from CS.*
$\alpha$ — *Angle subtended by TC at P.*
*W — Width of horn mouth—32 cm. for all horns.*
a — *Slant length of the horn. (In these experiments* a *ranged from 176 to 25 cm.)*
b — *Distance S to T (the mean value of* b *in these experiments was 88.5 m.).*
$\lambda$ — *Wave length—3.2 cm.*

*In these experiments* b *is very large so that the following approximations are valid:*

$$\frac{b}{a+b} \doteqdot 1; \quad \phi \doteqdot \alpha; \quad \overline{TC} \doteqdot a\phi; \quad \overline{TU} \doteqdot \frac{W}{2} - a\phi; \quad \overline{TR} \doteqdot \frac{W}{2} + a\phi$$

length of the horn from its vertex. In the illustration it has been rotated through an angle $\phi$ so that a ray from the source, $S$, directed at the vertex of the horn, $P$, meets the equiphase locus $UTCR$ at $T$, which is then the pole of the system. According to well known theory (5, p. 228) one can write:

$$|E|^2 = \frac{ab\lambda}{2\,(a+b)}\left[\left\{\int_{-V_1}^{V_2}\cos\frac{\pi v^2}{2}\,dv\right\}^2 + \left\{\int_{-V_1}^{V_2}\sin\frac{\pi v^2}{2}\,dv\right\}^2\right].$$

In these relations,

$|E|$ = the absolute value of the electric field strength;

$a$ = the slant length of the horn from mouth to vertex;

$b$ = the distance from the source to the pole of the system;

$\lambda$ = wave length of the radiation;

$W$ = width of the horn mouth, here taken equal to the arc $UTCR$ as a convenient approximation;

$$V_2 = \sqrt{\frac{2(a+b)}{ab\lambda}}\cdot\overline{TU} \qquad V_1 = \sqrt{\frac{2(a+b)}{ab\lambda}}\cdot\overline{TR}$$

When radiation patterns are measured, the source, $S$, is made very distant so that all rays from the source are approximately parallel at the mouth of the horn. Then

$$b \longrightarrow \infty\,, \qquad \frac{b}{a+b} \doteqdot 1 \qquad \text{and } \phi \doteqdot \alpha\,,$$

so that $\overline{TC} = \alpha a = \phi a$, $\overline{TR} = \left(\frac{W}{2} + a\phi\right)$ and $\overline{TU} = \left(\frac{W}{2} - a\phi\right)$.

With these changes $\frac{ab\lambda}{2(a+b)}$ becomes approximately $\frac{a\lambda}{2}$ and the limits take on the simple forms:

$$V_2 = \sqrt{\frac{2}{a\lambda}}\left(\frac{W}{2} - a\phi\right) = \sqrt{\frac{2a}{\lambda}}\left(\frac{W}{2a} - \phi\right),$$

$$V_1 = \sqrt{\frac{2}{a\lambda}}\left(\frac{W}{2} + a\phi\right) = \sqrt{\frac{2a}{\lambda}}\left(\frac{W}{2a} + \phi\right).$$

Since the wave guide at the throat of the horn imposes a sinusoidal variation on the amplitude of the received radiation in the $H$-plane and since the Fresnel integrals imply uniform field across the aperture, this method can be used to calculate $E$-plane patterns only.

The horns were measured by rotating them on a turntable, mounted about 15 ft. above the ground, in a location free of any obstruction, at a distance of 88.5 m. from the source of the 3.2 cm. waves. The distant source, $S$ (see Fig. 1), of the radiation consisted of a 3.2 cm. Shepherd klystron coupled through wave guide to a dipole array at the focus of a paraboloid mirror; the aperture of the mirror was chosen small enough to produce a uniform patch of nearly plane waves over the whole region in which the horn was rotated. The output of the klystron was square wave modulated at 150 c.p.s. The radiation was detected by a silicon crystal at the throat of the horn and the

modulation component passed on through a tuned amplifier stage to an attenuation box and thence to other tuned stages and an output meter. The noise bandwidth of the system was 8 c.p.s. and the whole system including the crystal was found to be linear with power over a range of 30 db.

At each change in the angle $\phi$ of 1° the attenuation box was adjusted to bring the output of the system to a standard value. The attenuation in decibels in each case was used as a measure of the relative power received.

## Results and Conclusions

All of the electromagnetic horns which were used in these experiments were built with the same aperture, 32 cm. square or 10λ at the operating wave length of 3.2 cm. The slant lengths, that is, the values for $a$ of the horns, are 176, 100, 47.5, and 25 cm. The horns are of approximately square cross section but all are subject in some measure to irregularities in construction which produce asymmetries in their radiation patterns. Measurement shows a slight departure from the assumed constant field at the horn mouth in the $E$-plane of the longer horns and a pronounced departure in the shortest, 25 cm. horn; it is assumed that these irregularities are due to horn modes other than the $TE_{01}$ generated by discontinuities at the horn throat.

Figs. 2, 3, 4, and 5 are the $E$-plane radiation patterns of the horns; both measured and calculated values of relative power at the horn throat are plotted in these graphs as a function of the angular displacement of the horn from the line joining horn and source. Of all the measured patterns that for the shortest horn alone bears no relation to the predicted values; in view of the probable presence of other modes this is not conclusive evidence of the complete failure of the Kirchhoff approximations at a distance appropriate to the length and aperture of this horn. The figures show that measured and predicted values are in agreement up to an angular displacement of 15° or ¼ radian for horns as short as 50 cm. (16 wave lengths); there is some evidence that for horns longer than 50 cm. even the minor disagreements within the ¼ radian limit are due to horn asymmetries rather than to failure of the optical theory.

---

FIG. 2. *Measured and calculated radiation patterns of a rectangular horn radiator.*
*Rotation is in the plane of the electric vector.*
*The slant length of the horn (dimension* a *of Fig. 1) is 176 cm.*
*The aperture of the horn is 10 wave lengths square = 32 cm.*
*Wave length = 3.2 cm.*
*Theoretical values* ——— *Measured values* + ——— + ———

FIG. 3. *Measured and calculated radiation patterns of a rectangular horn radiator.*
*Rotation is in the plane of the electric vector.*
*The slant length of the horn (dimension* a *of Fig. 1) is 100 cm.*
*The aperture of the horn is 10 wave lengths square = 32 cm.*
*Wave length = 3.2 cm.*
*Theoretical values* ——— *Measured values* + ——— + ———

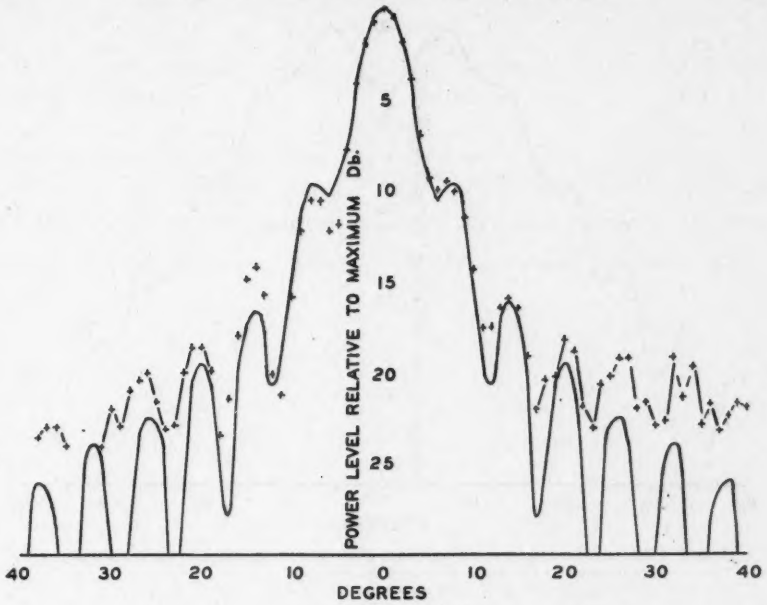

POWER LEVEL RELATIVE TO MAXIMUM Db.
5
10
15
20
25
40
30
20
10
0
10
20
30
40
DEGREES

FIG. 2.

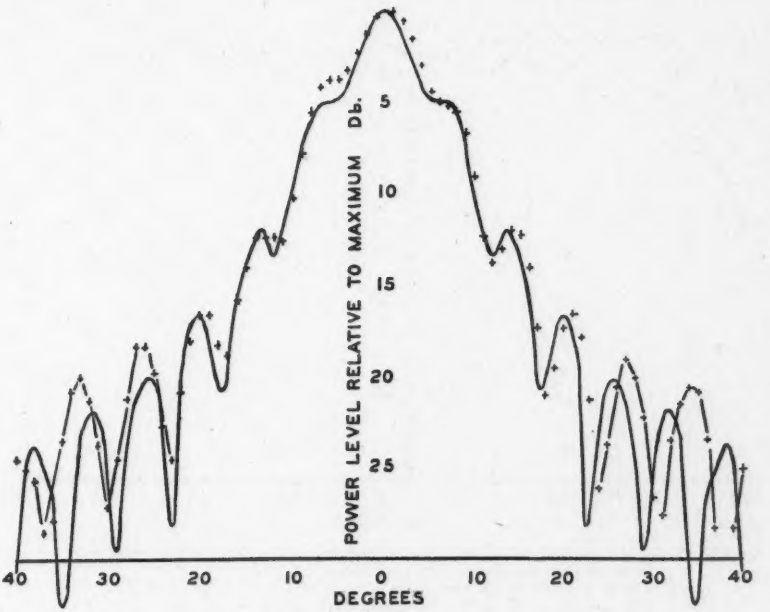

POWER LEVEL RELATIVE TO MAXIMUM Db.
5
10
15
20
25
40
30
20
10
0
10
20
30
40
DEGREES

FIG. 3.

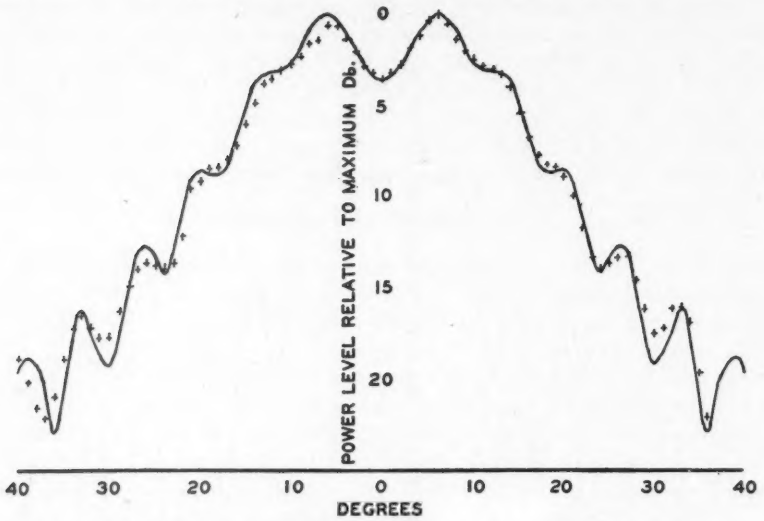



FIG. 4. *Measured and calculated radiation patterns of a rectangular horn radiator.*
*Rotation is in the plane of the electric vector.*
*The slant length of the horn (dimension* a *of Fig. 1) is 47.5 cm.*
*The aperture of the horn is 10 wave lengths square = 32 cm.*
*Wave length = 3.2 cm.*
*Theoretical values* ——— *Measured values* + ——— + ———

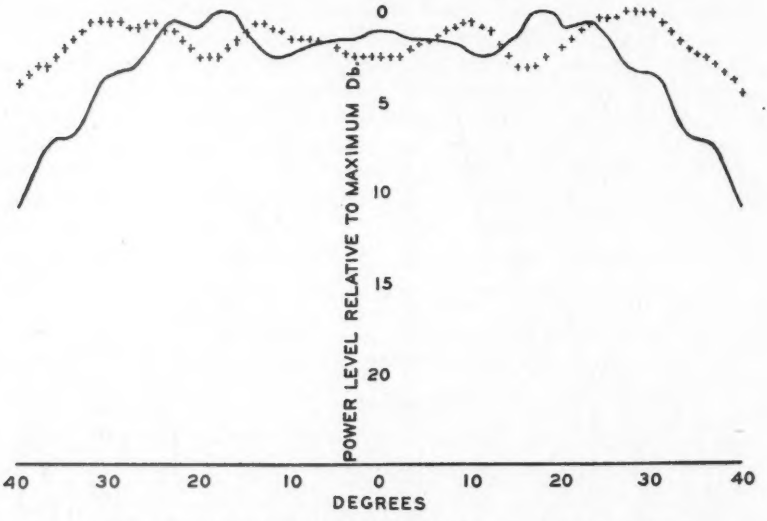



FIG. 5. *Measured and calculated radiation patterns of a rectangular horn radiator.*
*Rotation is in the plane of the electric vector.*
*The slant length of the horn (dimension* a *of Fig. 1) is 25.0 cm.*
*The aperture of the horn is 10 wave lengths square = 32 cm.*
*Wave length = 3.2 cm.*
*Theoretical values* ——— *Measured values* + ——— + ———

## Acknowledgment

This research was made possible by a grant from the National Research Council of Canada.

## References

1. BARROW, W. L. and CHU, L. J. Proc. Inst. Radio Engrs. 27 : 51-64. 1939.
2. BARROW, W. L. and GREENE, F. M. Proc. Inst. Radio Engrs. 26 : 1498-1519. 1938.
3. CHU, L. J. J. Applied Phys. 11 : 603-610. 1940.
4. SCHELKUNOFF, S. A. Electromagnetic waves. D. Van Nostrand Company, Inc., New York. 1943.
5. WOOD, R. W. Physical optics. 3rd ed. The Macmillan Company, New York. 1934.

# THE USE OF DIAPHRAGMS IN THE ELECTRON MICROSCOPE[1]

By S. G. Ellis[2]


## Abstract

A method is described for deducing electron trajectories from optical measurements made on the electron microscope. A device for centring and changing apertures while the microscope is in operation is described. The choice of the size and position for diaphragms is discussed, together with other factors involved in their use.


Diaphragms, when used in the electron microscope, act either as field limiting or aperture limiting diaphragms. The objective diaphragm acts as an aperture limiting diaphragm by removing from the beam leaving the specimen electrons whose trajectories made more than a certain angle $\alpha_0$ with the axis of the lens at the specimeh. This angle $\alpha_0$ is called the angular aperture of the lens. More precisely it may be called the physical angular aperture of the lens. The objective diaphragm will also prevent, to a certain extent, electrons from reaching the final image if they have been inelastically scattered by parts of the specimen not conjugate with that image. The objective diaphragm therefore increases the contrast in the final image, and in principle might be expected to increase the resolution in micrographs.

## Theory of Diaphragm Sizes and Positions

When the 1944 Toronto electron microscope (2) was constructed, provision was made for putting diaphragms in the three magnetic lenses at any point on the axis and for centring the diaphragms while the microscope was in operation. The design of this microscope was made by Drs. L. Newman and J. H. L. Watson (12). It fell to the writer to determine the best sizes and axial positions for the diaphragms. It was evident that the solution of this problem depended on discovering the electron trajectories in the lenses.

From the work of Dosse (3) it was known that the axial field of an objective lens with two identical pole pieces could be described with fair accuracy by the empirical formula

$$H = H_0/(1 + z^2/a^2) \ . \qquad (1)$$

Here, an $Oz$ axis has been chosen, positive in the direction of electron motion, and with origin at the field maximum. $H_0$ is the maximum axial magnetic field, and $a$ is the distance along the axis at which the field falls to $H_0/2$.

Glaser had solved the paraxial ray equation for this field distribution and had given a very complete account of the optics of the lens (4).

[1] *Manuscript received June 27, 1947.*
*Contribution from the Department of Physics, University of Toronto, Toronto, Ont.*

[2] *Research Assistant and Lecturer. Holder of a Fellowship under the National Research Council of Canada, 1945-1946. Now at RCA Laboratories, Princeton, N. J.*

If $r$ is the radial displacement of the electron, the general solution of the paraxial ray equation for the above field is,

$$r = a[1 + z^2/a^2]^{\frac{1}{2}} \{ C_1 \sin ([1 + k^2]^{\frac{1}{2}} \operatorname{arccot} z/a) + C_2 \cos ([1 + k^2]^{\frac{1}{2}} \operatorname{arccot} z/a) \} , \quad (2)$$

where $$k^2 = - \frac{eH_0^2a^2}{8mV} , \quad (3)$$

$V$ = speed of the electrons in electron volts,

$e$ = charge of electron,

$m$ = mass of electron.

Marton and Hutter (10) have used this equation in a discussion of the optimum size and position for an objective diaphragm. Briefly, they determine the path of an electron leaving the centre of the specimen at a supposedly optimum angular aperture, after elastic collision with the specimen. They recommend that a diaphragm be placed in the plane where the radial displacement of such an electron reaches a maximum value ($r_0''$ say) and that the diaphragm have this radius $r_0''$.

Two objections may be raised to this theory. In the first place such a diaphragm would exert an aperture limiting effect on electrons proceeding from the periphery of that part of the specimen imaged on the photographic plate, different from the effect on the electrons from the centre of the specimen. Second, the method of determining $H_0$ and $a$ is not clearly specified. The accurate determination of the axial field distribution is difficult because of the small size of the objective pole pieces, and the calculation of electron trajectories from such measurements notoriously inaccurate because of the cumulative nature of the errors (5). The method described below was evolved to obviate these difficulties.

If $u_0$ = distance from specimen to the origin at the field maximum,

$v_0$ = distance from the origin to the intermediate image, then it can be shown from Equation (2) that

$$\frac{1}{v_0} - \frac{1}{u_0} = \frac{1}{z_f} + \frac{a^2}{u_0 v_0 z_f} , \quad (4)$$

where

$$z_f = - a \cot (\pi/[1 + k^2]^{\frac{1}{2}}) , \quad (5)$$

the sign convention introduced above being maintained. Further, the magnification $M_0$ is given by

$$M_0 = - \left[\frac{a^2 + v_0^2}{a^2 + u_0^2}\right]^{\frac{1}{2}} , \quad (6)$$

the minus sign indicating inversion of the image in the meridional plane. It is supposed here that

$$1 < [1 + k^2]^{\frac{1}{2}} < 2 .$$

If the position of the field maximum can be estimated from the pole piece configuration, and $u_0$, $v_0$, and $M_0$ are measured for the objective*, $a$ can be calculated from Equation (6), $z_f$ from Equation (4), and then $[1 + k^2]^{\frac{1}{2}}$ from Equation (5).

If the pole pieces of the objective are not identical, or if for any other reason the position of the maximum axial field is uncertain, the following procedure may be employed.

Let $u_0'$ be the distance from the object to some arbitrarily chosen level, such, for example, as the upper surface of the upper pole piece. Then

$$u_0 = u_0' + z'$$

and

$$M_0 = -\left[\frac{v_0^2}{a^2 + (u_0' + z')^2}\right]^{\frac{1}{2}}, \tag{7}$$

neglecting $a$ in comparison with $v_0$.

Then

$$\left(\frac{v_0^2}{M_0^2} - u_0'^2\right) = 2z'\,u_0' + (a^2 + z'^2)\,. \tag{8}$$

Plotting $\left(\frac{v_0^2}{M_0^2} - u_0'^2\right)$ against $u_0'$ for different values of the latter, a straight line will be obtained if the range of objective currents is small enough that $a$ remains unchanged. The slope of the line is $2z'$ and its intercept $(a^2 + z'^2)$, from which $a$ may be found.

The numerical calculation of the trajectory is facilitated by rewriting Equation (2) in the form

$$y = [1 + x^2]^{\frac{1}{2}} A \sin(\omega\,\theta + \epsilon)\,, \tag{9}$$

where $x = z/a$

$$y = r/a$$

$$\theta = \operatorname{arccot} z/a$$

$$\omega = [1 + k^2]^{\frac{1}{2}}\,. \tag{10}$$

The angular aperture of the lens is

$$\alpha = \frac{dr}{dz} = \frac{dy}{dx}$$

measured at the object, where

$$\frac{dy}{dx} = [1 + x^2]^{-\frac{1}{2}} \cdot [x\,A \sin(\omega\,\theta + \epsilon) - \omega\,A \cos(\omega\,\theta + \epsilon)]\,. \tag{11}$$

For any assumed value of the aperture, the values of $r$, $z$, and $\alpha_0$ at the specimen may be substituted in Equations (9) and (11), and the specific values of $A$ and $\epsilon$ deduced. Corresponding values of $x$ and $y$ for $z$ in the range

$$u < z < 2\,z_f$$

can be calculated, the trajectories plotted, and the axes converted to values of $r$ and $z$. This has been done in Figs. 1 and 2 for an objective used in the

** The intermediate image is usually formed below the intermediate screen, a fact which must be kept in mind if magnification measurements are made at the intermediate screen.*

1944 Toronto microscope. In effect, trajectories of the form given by Equation (2) have been fitted to the known initial and final trajectories for the objective.

It is seen in Figs. 1 and 2 that the trajectories pass through an exit pupil or crossover at $z = 0.4$ cm. and that a diaphragm placed there will exert the same aperture limiting effect on electrons from all of the observed parts of

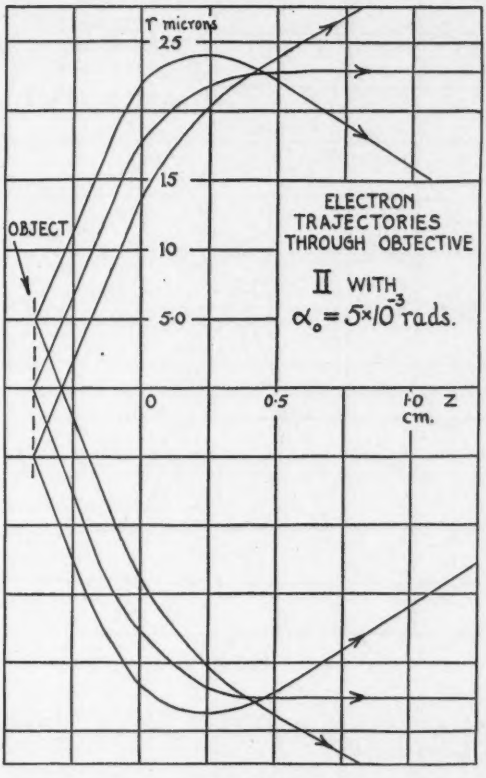



FIG. 1.

the specimen. It may be mentioned that for the trajectories shown in Figs. 1 and 2 the aperture $\frac{dr}{dz}$ at $z = u$ is 2% greater than at $z = -\infty$. That is, the field of this objective does not exert a noticeable converging effect on the illuminating beam.

The radius of the diaphragm depends on the angular aperture at which it is desired to operate the objective. A number of courses are open. For example, the angular aperture may be made equal to the maximum angular

aperture of the illuminating beam. This will permit focusing with a smaller depth of field than that used in making micrographs. Another course is to make the physical aperture equal to the calculated optimum angular aperture. At present, however, decisive experimental proof of the existence of an

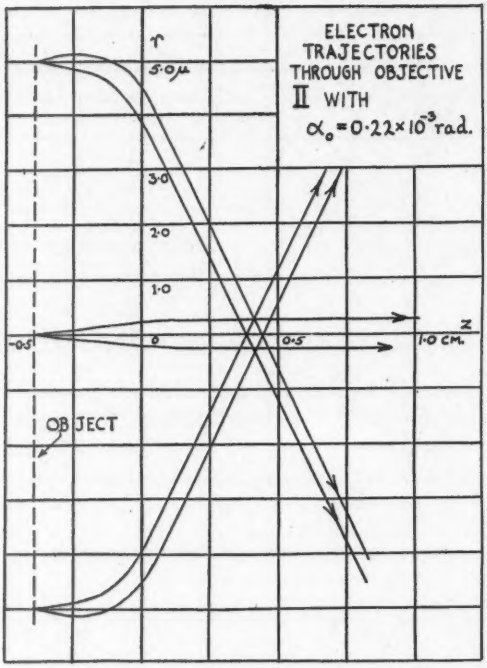



FIG. 2.

optimum angular aperture, as predicted by theory, is lacking. So long as the diaphragm is used primarily to increase contrast, the size of the diaphragm is not too critical, and the latter course mentioned above will lead to an acceptable solution.

## Choice of Angular Aperture

The optimum angular aperture $\alpha_{OPT}$ is usually calculated by combining the diffraction defect $\delta_{DIFF}$ and the spherical aberration defect $\delta_{SPH}$ either arithmetically

$$\delta = \delta_{DIFF} + \delta_{SPH}\,, \tag{12}$$

or by the error law

$$\delta = (\delta^2_{DIFF} + \delta^2_{SPH})^{\frac{1}{2}}\,. \tag{13}$$

If $C_{SPH}$ is the spherical aberration coefficient of the objective then

$$\delta_{SPH} = C_{SPH}\,\alpha^3 \tag{14}$$

and

$$\delta_{DIFF} \doteq \lambda/2\,\alpha\,, \tag{15}$$

where $\lambda$ is the de Broglie wave length of the illuminating electrons. When $a$ and $k^2$ are known, the coefficient $C_{SPH}$ can be estimated from the formula given by Glaser (4). Fig. 3 shows the variation of $\delta$ with $\alpha$ according to Equations (12) and (13) for an objective used in this laboratory. This

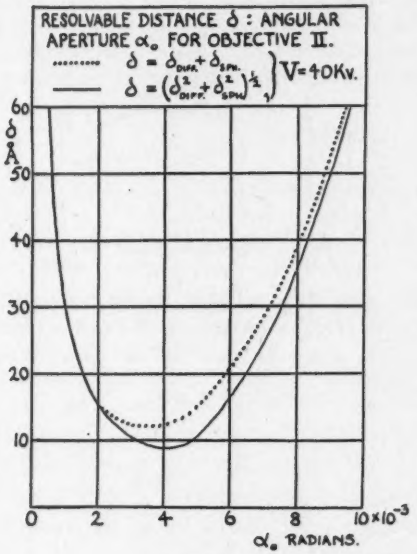



FIG. 3.

indicates that for $\alpha$ between 2 and 6 $\times$ $10^{-3}$ the calculated resolving power of the microscope is less than 20 Å. In other words, a 50 $\mu$ diameter diaphragm should be suitable for such a lens if one wished to attain the highest resolution in examining thin specimens with well defined variations in mass thickness.

With thicker specimens, the value of $\alpha_{OPT}$ will differ from that given above, yet in practice a diaphragm chosen on the above considerations will prove a suitable compromise.

With many specimens the effective resolution is conditioned by contrast limitations in the image caused by the fact that different parts of the specimen have little difference in electron scattering power. It should be noticed, however, that the inner potential of the specimen may contribute effects that tend to enhance the contrast in the image.

Consider, for example, a specimen in the form of a film with surfaces that have concave and convex parts. Such a specimen is shown in section in Fig. 4. For our present purposes it is sufficient if the equipotentials showing

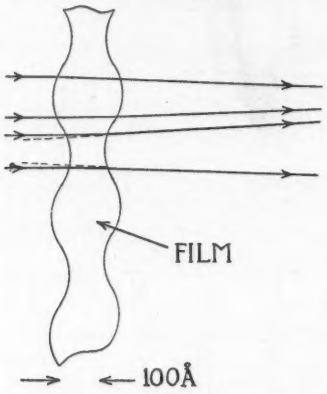



FIG. 4. *Refraction in thin film.*

the transition to the inner potential have the form shown in the figure. Let the radius of curvature of these surfaces be $R$ and the inner potential be $V_i$. If biconvex parts of the film exist they will act as a converging lens on the electrons of focal length

$$f_i = VR/V_i . \tag{16}$$

For $V_i = 10$ v., $V = 50$ kv., and $R = 100$Å, $f_i = 50\ \mu$. If then the objective is underfocused (objective current low) by 50 $\mu$, bright regions will be formed in the image at points conjugate to biconcavities in the film; or if overfocused by 50 $\mu$—at points conjugate to biconvexities.* The in-focus image should show less contrast.

If one wishes to gain information about the specimen by employing this effect it would seem desirable to employ the smallest aperture that will still permit adequate resolution according to Equation (15). For in this way the confusing effect of the scattered electrons, reasonably uniform for the whole specimen, will be avoided and the refraction effect enhanced in comparison.

It may be noted here that the objective diaphragm size and position may be determined rapidly by the following approximate method. If $\alpha_0$ is the maximum angular aperture to be permitted for the objective, the diaphragm radius $r_0''$ is given approximately by

$$r_0'' = \alpha_0 f = \alpha_0 (a^2 + z_f^2)^{\frac{1}{2}} . \tag{17}$$

The diaphragm may be placed at a distance $z_f$ below the centre of the lens.

* *It is possible that some of the contrast in Fig. 2, reference (9), is due to this effect.*

Since the condenser lens may be treated as a thin lens, and since the electron trajectories near the lens are effectively parallel to the axis, the diaphragm radius can be calculated from

$$r_c'' = v_c \alpha_c \text{ (max)},$$

where $\alpha_c$ (max.) = maximum angular aperture of the illuminating beam,

$v_c$ = distance from the centre of the condenser lens to the specimen.

## Method of Manufacture

A steel needle is ground on a fine oilstone block until the point, viewed at ×100 in a light microscope, has the appearance shown in Fig. 5. To obtain a very fine point, the needle is held very obliquely to the surface of the oilstone and moved in the direction of its length. The needle is rotated during grinding to ensure that the point shall be free from flat surfaces. Abrasive is removed from the needle by dipping it in dilute nitric acid (one volume of concentrated acid to two volumes of distilled water), then washing in distilled water, and then scrubbing it with a lint-free lens paper.* This is a variation on a method first described by Hillier (6).




FIG. 5. *Profile of needle point for making diaphragms.*

The condenser diaphragm is made from 0.005 in. bronze sheet, and the objective diaphragm from 0.002 in. copper or brass foil. The diaphragm blank is cut to size with a suitable punch, flattened, and placed on a glass microscope slide. The holes are then gently drilled with a needle, using a rotary motion. In the case of the objective diaphragm one large hole (1 or 2 mm. diameter) is made with a punch and the smaller holes are drilled around it as shown in Fig. 6, *a* and *b*. Holes down to 30 μ diameter can be made in this way. With practice, holes down to 5 μ diameter can be produced.

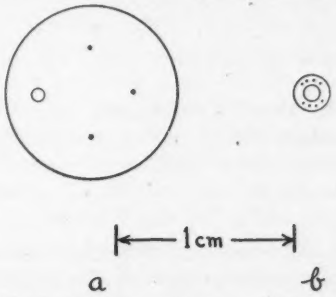



FIG. 6. *Two forms of objective diaphragm.*

* *Ross-Adams Lens Tissue is suitable.*

The finished diaphragm is cleaned by etching in dilute nitric acid and washing in distilled water. It can be dried on lint-free lens paper. Both sides of the diaphragm are then examined in a light microscope to ensure that it is free from dirt and lint. The diaphragm should be completed as shortly as possible before its inclusion in the microscope so that it is exposed to air-borne dust for the minimum time. The final test of the cleanliness of the diaphragm is made when the microscope is in operation.

A more elaborate arrangement for making diaphragms has been described by von Ardenne and Reibedanz (1).

## Method of Mounting

The diaphragm, *D* (Fig. 7), is mounted on the top of a brass chimney, *C*, which has a base, *B*, that bears on the lower surface of the lens. This base is held to the lens by a retaining ring, *P*. The chimney is moved, transversely

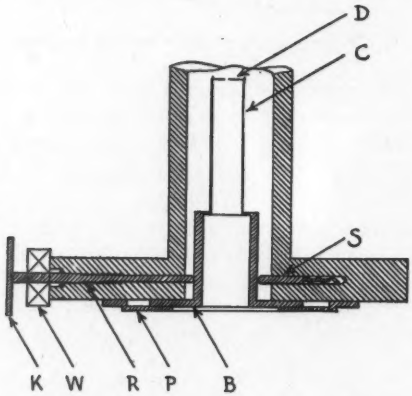



FIG. 7. *Diaphragm moving mechanism. Vertical centre section, not to scale.*

to the axis of the lens, by a rod, *R*, which has a threaded section, and is kept in contact with *B* by a sprung rod, *S*, bearing on the other side of the chimney. The rod, *R*, can be turned from outside the microscope by the knob, *K*, the Wilson seal, *W*, maintaining the vacuum (14). A similar rod for movement perpendicular to the plane of Fig. 7 is also provided.

Fig. 8 shows a detail of the top of a diaphragm chimney. In Fig. 8*a* the lower surface of the lower pole piece has been hollowed to permit the lateral movement of the diaphragm. The diaphragm in this case consists of one large hole (1 mm. diameter) and several smaller ones, as shown in Fig. 6*a*. The diaphragm is held to the chimney by a retaining ring. In Fig. 8*b*, which shows a lens of shorter focal length, the diaphragm is soldered with Wood's metal to two wires projecting from the top of the chimney. No flux is used in this soldering. Here the diaphragm is smaller but still consists of one large

hole surrounded by several smaller holes (Fig. 6*b*). Where the diaphragm is soldered to the supports, a final etching with nitric acid is done after the soldering is completed.

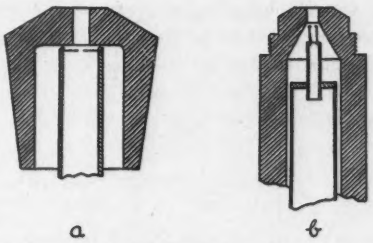



FIG. 8. *Diaphragms in position beneath lower pole piece of objectives.*

If the diaphragm is made large enough to accommodate several holes as shown in Fig. 6*a* then it will have to be situated somewhat below the exit pupil of the lens. In order that rays from the periphery of the field of view shall not be obstructed, the radius of the diaphragm hole has to be increased. If plots such as those shown in Figs. 1 and 2 have been made, the required diaphragm radius is readily determined. Alternatively, an approximate value for the diaphragm radius may be calculated from

$$r_0'' = \alpha_0 (a^2 + z_f^2)^{\frac{1}{2}} + r_0' (d + z_f)/z_f , \qquad (18)$$

where $r_0'$ = radius of that part of specimen that is to be imaged on the photographic plate,

$d$ = distance from lens centre to the diaphragm.

While the objective lens is removed from the column it is convenient to record the number of turns of the knobs, $K$ (Fig. 7), required to change from one hole to another of the diaphragm. It is very important that the large hole be sufficiently well centred by eye that the axis of the objective passes through it. If this condition is not observed, the intermediate screen may receive no electrons when the microscope is brought into operation, and the subsequent centring of the diaphragms and alignment of the lenses will be possible only if good fortune attends the attempt.

## Method of Centring

The condenser diaphragm is centred as accurately as possible by eye when it is introduced into the lens. The procedure for centring the condenser diaphragm can be best described with Fig. 9. With the diaphragm off the axis of the condenser lens the illumination, as viewed at the intermediate screen, follows a curved path as the condenser lens current is varied through the value giving the maximum aperture of illumination, i.e., varied through focus. With the condenser lens out of focus, the condenser diaphragm is moved until the enlarged area of illumination on the intermediate screen is

concentric with the position of the in-focus area of illumination. If the plane of the condenser diaphragm is not in the plane of the condenser lens centre, the above adjustment may have to be repeated after the usual procedure for aligning the illuminating system of the microscope has been performed. The centring of the condenser diaphragm can easily be done with a specimen in the microscope.

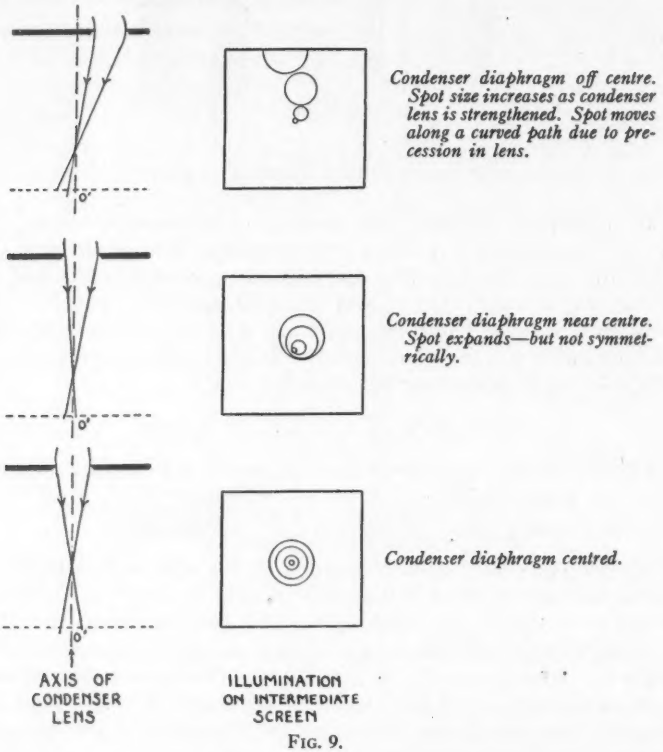



FIG. 9.

To centre one of the small holes in the objective diaphragm, the knobs, $K$ (Fig. 7), are turned the appropriate number of revolutions as previously determined when the lens was removed from the column. This will generally bring the hole near to but not on to the axis of the lens. Since the exit pupil of the objective is about 50 $\mu$, or less, in diameter (See Figs. 1 and 2) it will act as a nearly point source of electrons, and if the diaphragm is $d$ cm. below the exit pupil, will throw a shadow image of the diaphragm on the intermediate screen. The magnification $M_0'$ of this image will be given by

$$M_0' = \frac{v_0 - z_f}{d} \doteq \frac{v_0}{d}. \qquad (19)$$

Equation (19) provides an independent method for checking the accuracy of the measurement of $z_f$, since it permits the calculation of the position of the exit pupil when $M_0'$ and $v_0$ are known. For objectives in which the two pole pieces do not have the same form, Equation (19) provides the most accurate method of finding the position of the exit pupil. The diaphragm is next moved carefully until the shadow image of the hole coincides with the hole in the intermediate screen. This adjustment is easier if the condenser is out of focus, so that a large area of the intermediate screen is illuminated.

Dark field observation can be obtained by moving the objective diaphragm transversely as shown in Fig. 10, so that only scattered electrons can pass through to form the final image.

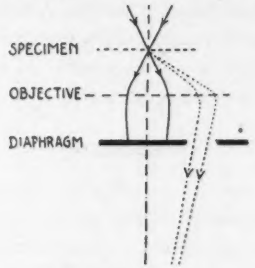



FIG. 10. *Objective diaphragm moved sideways so as to pass only scattered electrons and give dark field observation.*

A final check on the cleanliness of the diaphragm can be made by making a double exposure and moving the diaphragm a small distance (less than $r_0''$) sideways between the exposures. Under these conditions non-conducting bodies on the diaphragm will be charged to different amounts, producing image shifts, so that doubling of the image will appear in the doubly exposed plate.

In one method of using the 1944 Toronto electron microscope as an electron diffraction camera, the specimen is placed close below the projector lens. It is desirable to delimit the electron beam so that it will not strike the projector pole faces and also to decrease the effect of spherical aberration in the projector lens. This can be achieved by placing a diaphragm above the objective in the specimen cartridge. It can be centred by the object moving screws.

The radius of the beam at the projector pole pieces will be approximately $r_0'' v_0/u_0$, where $r_0''$ is the diaphragm radius. It is therefore advantageous to make $u_0$ large in this case in order that $r_0''$ shall not have to be very small.

## Observations

The most noticeable effect of the objective diaphragm is to increase the contrast in the image. A 50 $\mu$ diameter diaphragm has been customarily used in the 1944 Toronto microscope. This diaphragm has aided in the

examination of thick specimens and also specimens such as Formvar replicas, and soaps (without shadow casting) in which the contrast is low.

It cannot be said from the results obtained that the objective diaphragm has led to an increase in resolution. However, the instrument resolving power has been limited by lack of symmetry in the field of the objective and by the difficulty of obtaining exact focus, so that the above point remains undecided.

Dark field observation by the method shown above does not produce good resolution. This is in part due to the large chromatic error with the scattered electrons and in part due to the non-symmetric nature of the imaging beam. Dark field observation does, however, provide a sensitive method of observing the Bragg reflections from crystalline bodies if the diaphragm is so situated as to pass only the diffracted beam. This then provides a sensitive method for detecting small crystals in the specimen. Dark field observation also provides a method of observing qualitatively the scattering power of the specimen.

## Discussion

Some objections to the use of an objective diaphragm have been raised. Since the diaphragm is grounded to the body of the microscope, charges will be induced upon it that will deflect those electrons passing close to the diaphragm. While a precise mathematical treatment of the problem is difficult, an approximate calculation (15, pp. 700-701) shows that the error introduced amounts to 10Å (when referred to the object) for electrons passing within 1 $\mu$ of the wall in a typical case. It should be mentioned, however, that less than 10% of the imaging electrons pass within 1 $\mu$ of the wall if the diaphragm radius is greater than 21 $\mu$ even when the current per unit solid angle leaving the object is independent of direction.

Another objection that has been made is that if the objective aperture is made considerably less than the maximum aperture of the illumination, then the depth of focus does not decrease when the aperture of the illumination is brought to its maximum value as much as it would if $\alpha_0$ was not defined by a diaphragm. As a consequence of this the visual focusing is made more difficult. This objection carries less weight now that electron microscopes can be focused at reduced aperture (8).

Finally, Hillier (7) has pointed out that a diaphragm situated at the exit pupil of the objective is in a position of maximum current density and that polarizing layers (11, 13) will form on the diaphragm, charge up from the electron beam, and lead to a decrease in the resolution by deflecting the imaging electrons. These polarization layers have been observed on diaphragms removed from the Toronto microscope. However, with several small holes in the diaphragm it is easy to change to a clean one if it is needed, and in any case the large hole, 1 mm. diameter, in the diaphragm can be used if any disturbing effect, either from polarizing layers or induced charge, is suspected.

It may be mentioned that the effect of the induced charges noted above is in opposition to the effect of the spherical aberration of the objective. In principle then, the spherical aberration of the objective could be corrected if a diaphragm at the exit pupil exerted on the electrons passing through it a centrifugal impulse proportional to the cube of their radial displacement up to a certain limiting value, and completely blocked electrons of greater radial displacement. It is evident that the design and construction of such a diaphragm would introduce very considerable difficulties and might well be unjustified by the ends to be secured.

Hillier (9) has described an objective using two components. The first is a weak lens giving approximately unit magnification, the second is a conventional objective of short focal length. Fig. 11 shows the approximate electron trajectories through such a lens for $\alpha_0 = 5 \times 10^{-3}$. It will be seen that a

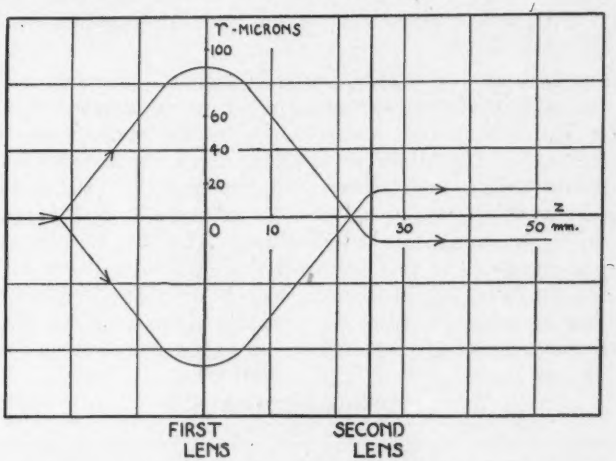



FIG. 11. *Approximate electron trajectories through double objective described by Hillier (9).*

diaphragm placed in the first component could have a diameter of nearly 200 $\mu$ and still exert the same limiting effect as a 30 $\mu$ diameter diaphragm in the second component. Moreover, by considering the paths of rays from the periphery of the specimen area examined it will be seen that the axial position of the diaphragm is not critical when considered in terms of its field limiting effect. Hillier reports, however, that a diaphragm when used in this lens causes asymmetries in the image. If, to consider a simple case, the disturbing effect of a diaphragm is to cause a deviation, $\theta$, in a marginal ray, irrespective of which component the diaphragm is in, then its effect on the intermediate image is greater by a factor $2f_1/f_2$ if it is placed in the first component. Here $f_1$ is the focal length of the first component and $f_2$ that of the second. In so far as the disturbing effects are caused by the charging up of dust or polarizing

layers by scattered electrons, the deviation $\theta$ will be less for a given particle of dirt and a given ray with the dirt on a diaphragm in the first component. This is because the current density at the midplane of the first component is less than at the second component. The net result is that from the point of view of disturbing effects on the beam there is little difference between the two positions of the diaphragm.* Despite the greater spherical and chromatic aberrations of this system, this lens has the notable advantages of a greater working distance and a larger diaphragm size. The micrographs published by Hillier attest its virtues.

## Conclusions

Experience gained over the last three years with objective diaphragms in the 1944 electron microscope has led to the conclusion that despite their defects they are of great assistance in the examination of samples giving low contrast. With some samples their use has been imperative in visual observation and choice of field.

Now that high resolution micrographs of samples possessing well defined spacial variations of electron scattering power can be consistently produced, it will be important to try to improve the resolution when working with samples such as bacteria and viruses in which the various parts of the structure do not differ greatly in their ability to scatter electrons. For this reason it seems desirable to investigate further the influence of diaphragms on the resolution. If the cleanliness of the diaphragm is found to be a limiting factor then a mechanism such as that described above will be one way of providing a clean diaphragm whenever critical work is encountered. Alternatively, progress may be made only when the formation of the polarizing layers noted above can be suppressed, or when they can be removed from the diaphragm by heating it *in situ*.

## Acknowledgments

The author wishes to express his gratitude to Prof. E. F. Burton of the McLennan Laboratory for encouragement during the prosecution of this work, and to the National Research Council of Canada for a Fellowship.

## References

1. ARDENNE, M. v. and REIBEDANZ, H. Z. Instrumentenk. 60 : 22-26. 1940.
2. BURTON, E. F. and KOHL, W. H. The electron microscope; an introduction to its fundamental principles and applications. 2nd ed. Reinhold Publishing Corporation New York. 1946.
3. DOSSE, J. Z. Physik, 117 : 437-443. 1941.
4. GLASER, W. Z. Physik, 117 : 285-315. 1941.
5. GODDARD, L. S. and KLEMPERER, O. Proc. Phys. Soc., London, 56 : 378-396. 1944.
6. HILLIER, J. Ph.D. Thesis, University of Toronto. 1941.
7. HILLIER, J. Private communication.
8. HILLIER, J. J. Applied Phys. 17 : 307-309. 1946.
9. HILLIER, J. R.C.A. Rev. VIII : 29-42. 1947.

** I am indebted to Dr. Hillier for a discussion of the effects of contamination in this lens.*

10. MARTON, L. and HUTTER, R. G. E. Phys. Rev. 65 : 161-167. 1944.
11. STEWART, R. L. Phys. Rev. 45 : 488-490. 1934.
12. WATSON, J. H. L. Ph.D. Thesis, University of Toronto. 1943.
13. WATSON, J. H. L. J. Applied Phys. 18 : 153-161. 1947.
14. WILSON, R. R. Rev. Sci. Instruments, 12 : 91-93. 1941.
15. ZWORYKIN, V. K., MORTON, G. A., RAMBERG, E. G., HILLIER, J., and VANCE, A. W. Electron optics and the electron microscope. John Wiley & Sons, Inc., New York, and Chapman & Hall, Ltd., London. 1945.

# A LOW-PRESSURE GLOW-DISCHARGE PROTON SOURCE[1]

By Paul Lorrain[2]

## Abstract

A cold cathode proton source operating at about 200 v. at a pressure of a few microns is described. The discharge is essentially similar to that of a Philips vacuum gauge. The characteristics of the discharge, the ion extraction, and the proton production have been investigated. The addition of 10% of oxygen to the hydrogen increased the proton content of the ion beam from 10 to 50% while introducing only about 1% of oxygen and other foreign ions. The ionization processes are discussed.

## Introduction

The problem of the positive ion source for ion accelerators, and in particular of the proton source, has been stated by a number of authors (1, 5, 7, 13, 17, 21, 33, 36, 41, 42). It will suffice here to enumerate the desirable characteristics for such a source. They are: (*a*) ion beam current of the order of 1 ma. or more, depending on the accelerator, beam cross section of the order of 10 sq. mm., and low angular spread; (*b*) low energy spread in the ion beam; (*c*) high percentage of atomic ions; (*d*) low gas flow from the ion source to the accelerator; (*e*) small size; (*f*) low power dissipation; (*g*) stability, simplicity of operation and of power supplies. The relative importance of these characteristics depends on the accelerator and on the measurements contemplated.

For simplicity of operation, it is important that the source should not require a heated filament because (*a*) the filament is gradually destroyed by the positive ion bombardment and has a life span at most of the order of 100 hr., and (*b*) a filament power supply is required. Since the filament of a cyclotron ion source must be operated perpendicularly to a high magnetic field, it is usually heated with a high frequency current to reduce the mechanical strain, and the power supply required is elaborate and expensive. Most positive ion sources require a heated filament. The high voltage canal ray tube (7), the F. M. Penning (32), and the T. Franzini sources (14, 15, 19) are notable exceptions.

The type of discharge used in the present source appears to have been originated by L. R. Maxwell in 1931 (28). In his discharge, the electron path length from cathode to anode, and thus the number of ion pairs produced per electron emitted at the cathode, at low pressure, was multiplied by a large factor through electron oscillations. In this way, a low voltage discharge could be maintained even at very low pressures when the mean free path of the electrons for ionization was much larger than the dimensions of the discharge tube. Fig. 1 shows a schematic diagram of the Maxwell source.

[1] *Manuscript received June 13, 1947.*

*This work was performed partly at the Montreal Laboratory of the National Research Council and partly in the* Département de Physique *of the* Université Laval, *Quebec, Canada. Issued as N.R.C. No. 1629.*

[2] *Physicist. Present address: Physics Department, Cornell University, Ithaca, N.Y., U.S.A.*

A heated filament, $F$, was used as cathode and a plate, $P$, pierced with a hole opposite the filament, was used as anode. Parallel to the anode and on the side opposite to that of the filament was a second similar plate, $Q$, negative




FIG. 1. *The Maxwell source.*

with respect to the anode. The electrons emitted by the filament were focused by a powerful axial magnetic field through the hole in the anode and reflected back to the filament by the second plate. The electrons were again reflected at the filament and thus described a large number of oscillations before reaching the anode. Positive ions were collected on a third parallel plate, $R$, through a hole in the second plate, $Q$. This source could produce 3 ma. of positive ions at a pressure of 3 $\mu$, which is excellent, even today. It does not seem to have attracted much attention, however, probably because it required a magnetic field of 12,000 gauss and because the ions were collected immediately behind the second plate and were not available as a beam. Also, at the time, positive ion sources were of much less interest than they are today.

In 1937, F. M. Penning investigated two different types of low-pressure glow discharges in which electrons were made to oscillate in a magnetic field. One type was the 'inverted magnetron' (30). The other was essentially similar to L. R. Maxwell's source, but operated with a cold cathode. Using this latter type, F. M. Penning designed a vacuum gauge, now known as the Philips gauge (31), and an ion source (32). The discharge for his ion source occurred between three parallel plates, the two outside ones being the cathodes and the centre one, with a hole in its centre, being the anode. The magnetic field was axial. Electrons described oscillations between the two cathodes along the magnetic lines of force. The ion beam emerged from a hole in one of the cathodes. F. M. Penning's original paper seems to be the only one in the literature on this type of ion source. The operating voltage and the energy spread of the ion beam were very high, of the order of 10,000 v.

In 1940, A. T. Finkelstein (12) designed a source similar to that of Maxwell's, but operating at magnetic fields of a few hundred gauss and producing a maximum ion beam current of 150 ma. The operating voltage was low, about 50 v. This was followed in Germany by a number of similar sources (1, 2, 17, 41), notably those of M. von Ardenne (1, 2).

A. G. Ward, of the Montreal Laboratory of the National Research Council, undertook, in the spring of 1945, the design of a positive ion source of the Penning type for a Van de Graaff accelerator. With brass or steel electrodes, ion beam currents of 3.5 ma. were obtained at a pressure of 5 to 10 $\mu$ for a discharge current of 10 ma. and a discharge voltage of 1 to 2 kv. A later source gave ion beams of 100 to 150 $\mu$a. at 1 or 2 $\mu$ with 500 $\mu$a. and 5 kv. at the discharge. The main difficulties were the rapid variation of the source characteristics with pressure, the apparent existence of widely different modes of operation at a given pressure (42), and the fact that the proton percentage in the ion beam was unknown.

## I. Apparatus

### *1. The Vacuum System*

Fig. 2 shows the ion source and the mass spectrograph used. Fig. 11*a* shows a schematic diagram of the discharge tube. Electrolytic hydrogen, supplied in tanks by the Dominion Oxygen Company, Montreal, and containing 99.7% hydrogen and 0.3% oxygen, was piped through a copper tube and admitted to the system through a needle valve. The pressure in the hydrogen line was kept slightly above the atmospheric pressure to avoid the possible introduction of air. Water and other vapors could be added to the hydrogen by bubbling it in a flask near the needle valve. Hydrogen could be mixed with various percentages of oxygen by collecting the gases over water in an inverted beaker serving as a gasometer. The water was at room temperature. When pure hydrogen was required, the needle valve was replaced by a palladium diffusion tube (20).

An RCA 1946 thermocouple vacuum gauge and a Distillation Products VG-2 ionization vacuum gauge were used. The calibration of the thermocouple gauge was assumed to be the same for pure hydrogen and for the mixture of about 90% of hydrogen, 10% of oxygen, and 2% of water vapor which was used in the latter part of the work.

Fig. 2 shows the position of the gas inlet and of the vacuum gauges. The upper cathode, $K_1$, had holes around its circumference such that their aggregate pumping speed was much larger than that of the hole in $K_2$. The gauge pressure was thus approximately equal to that in the discharge. For small anode diameters, the pumping speed at $K_1$ was not sufficiently high and the gauge pressure was higher than the discharge pressure.

### *2. The Discharge Tube and the Beam Forming Lens*

The discharge tube was designed with the experimental work described below in mind. The cathodes, $K_1$ and $K_2$, and the anode, $A$, were made from 99.95% magnesium sticks supplied by Dominion Magnesium Limited, Toronto. The electrodes were supported on brass rings and glass spacers, and the whole was enclosed in a coaxial glass tube. $R$ was evacuated directly, as shown, and provided a low pressure region for the electrode leads. The brass rings supporting the electrodes were water cooled by means of loops of fine copper tubing replacing the wire leads shown in Fig. 2. This discharge

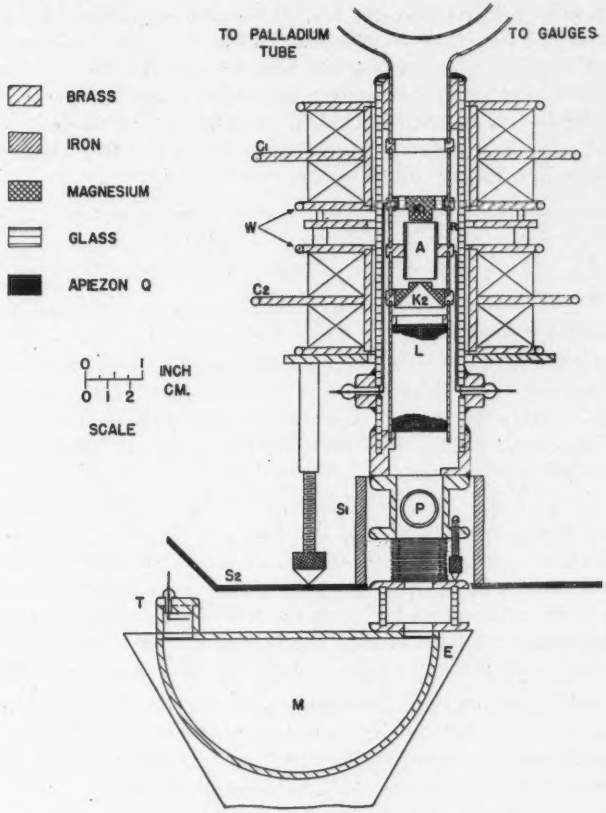



FIG. 2. *Ion source and mass spectrograph. $C_1$, $C_2$, coils for producing the magnetic field for the discharge; W, water cooling; A, anode; $K_1$, $K_2$, cathodes; R, low pressure region for the electrode leads; L, accelerating lens electrode; P, to pumps; M, mass spectrograph; $S_1$, $S_2$, magnetic shields; E, electromagnet pole piece; T, collector.*

tube was particularly convenient because: (*a*) dismantling or reassembling it involved only two Apiezon cement seals and thus required only a few minutes, (*b*) no trouble was experienced from spurious discharges at the leads, (*c*) the gauge pressure was approximately equal to the discharge pressure, and (*d*) the incoming gas was exposed only to glass and metal.

The cathodes were always the ones shown, but anodes of various diameters and lengths were used.

The electrodes, glass spacers, and brass rings were cleaned by dipping them for a fraction of a second in concentrated hydrochloric acid, rinsing in tap water and distilled water, and drying with alcohol. To avoid contact with the hands, the cleaned parts were assembled with a glass rod.

The magnetic field required for the discharge was produced by a pair of specially designed water cooled coils shown in Fig. 2. Each of the four sections was wound with 370 turns of No. 17½ B & S gauge HF Formex wire. The magnetic induction along the axis was calculated to be 129 gauss per amp. within ± 1% over a distance of 3.3 cm. on either side of the centre. These coils could operate continuously at magnetic fields of 1,000 gauss, and, for short periods, at fields up to 4,000 gauss.

The ions emerging from the lower cathode were formed into a beam by means of the electrostatic lens action of the lower conical surface of the cathode, $K_2$, and the cylinder, $L$. Accelerating voltages of about 5,000 v. were used.

*3. The Mass Spectrograph*

The mass spectrograph used was of the Dempster type (8) with an ion path radius of 6.0 cm. The ion energy was held constant and the magnetic field was varied to focus the various types of ions on the slit of the collector, $T$. Narrow slits, about 1/64 in. wide, were used so that the energy spread of the ion beam could be estimated.

To reduce secondary electron emission from the collector, it was biased at +300 v. with respect to the body of the mass spectrograph. Two iron blocks resting on the electromagnet pole pieces on either side of the collector provided a magnetic field which also served to reduce secondary emission. The variation of the collector current with the collector bias indicated that under these conditions secondary emission was negligible. The 300 v. bias actually had no appreciable effect on the percentage composition of the ion beam.

The curve of collector current against magnet current showed sharp maxima corresponding to the different types of ions in the beam. With the magnet current set for a maximum detector current, a change of about 1% in the former reduced the latter to one-half its maximum value.

The collector current was measured with a vacuum tube voltmeter with a full scale sensitivity of $1.33 \times 10^{-7}$ amp. on the lowest range. The ion beam currents used for the mass analyses were of the order of 500 $\mu$a.

The percentage composition of the ion beam under a given set of conditions was always determined two or three times in succession and the mean percentages were used. With pure hydrogen, a mass analysis could be reproduced from one day to another within approximately the experimental error. For example, the points shown on Fig. 5 were taken on two different days, both sets of points covering the whole range of pressure. When a mixture of hydrogen, oxygen, and water vapor was used, the reproducibility was not as good, but satisfactory. The points for any given curve were always determined in random order to eliminate any possible time variation in the composition of the ion beam.

Direct observation of the mass spectrum on an oscillograph screen was made possible in the following manner. The mass spectrograph magnetic field was swept automatically at a frequency of about 1 c.p.s. by opening and

closing the circuit of the electromagnet with a switch operated by an electric motor and a cam. This provided a satisfactory approximation of a saw-tooth sweep of the magnetic field because of the inductance of the electromagnet. The voltage across a resistance in series with the electromagnet provided a horizontal sweep for a DuMont type 208 oscillograph arranged for d-c. amplification. The current from the collector, $T$, was passed through a resistance of a few megohms and the voltage across this was fed to the $Y$-axis amplifier of the oscillograph. The oscillograph therefore displayed a graph of the detector current as a function of the magnetic field, i.e., the mass spectrum. The accuracy of this method is limited by: (*a*) unavoidable 'noise' in the discharge, producing rapid variations in the beam current; (*b*) non-linearity of the oscillograph response; (*c*) frequency dependence of the oscillograph response, since the sweep is not strictly saw-tooth and the peaks are not all swept at the same speed. The effect of (*a*) is reduced by taking the average heights of the peaks for a few sweeps; (*b*) and (*c*) are relatively negligible. The agreement between the oscillograph and the vacuum tube voltmeter results was within the experimental error. This method has the great advantage of providing a continuous indication of the ion beam composition. It was extremely useful, especially for rapid qualitative observations. It permitted direct observation of time variations in the beam composition, which would have been difficult to observe otherwise.

## II. Results

### *1. The Discharge*

The behavior of the discharge is highly satisfactory at pressures above a few microns; ignition is instantaneous and the operation is very reliable. The magnetic field does not need to be uniform or accurately axial, and can be supplied by a permanent magnet.

Magnesium was used for the cathodes because of its low work function and low sputtering, and also because of its availability and its machinability.

Cathodes of the shape shown in Fig. 2 concentrate positive ion bombardment of the cathodes and electron emission near the axis of the discharge. With flat cathodes, electrons emitted at their periphery reach the anode directly without oscillating and simply heat the anode without ionizing the gas. The green cathode light which is characteristic of magnesium (10) occurs only on that part of the cathodes that projects in the anode cylinder, except at high discharge currents.

It was observed that when the discharge was operated at potentials of the order of 1000 v., the anode material sputtered on to the cathode. It is thus desirable to use the same material for both the anode and cathode if such high discharge voltages are expected to occur.

The operation of the discharge was not changed appreciably when the anode was a ring instead of a cylinder as in Fig. 2. A cylindrical anode was used here because it lends itself to ion source designs which are mechanically very satisfactory.

With hydrogen, a bluish-white plasma fills the anode cylinder. There is no definite dark-space near the cathodes when magnesium is used, but with brass cathodes the plasma shows a definite convex surface facing the cathodes. With cathodes as in Fig. 2, the plasma is more luminous near the axis of the discharge tube. At very low pressures, of the order of 0.01 $\mu$, the luminous part of the discharge is a very fine line, about 1 mm. in diameter, along the axis of the discharge tube. With magnesium, the green cathode light is then concentrated in a small spot at the centre of the cathode.

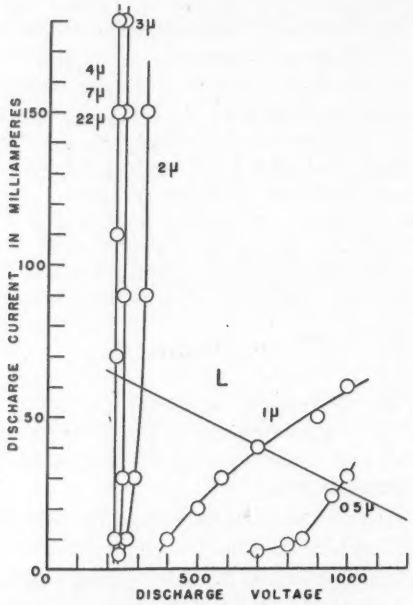



FIG. 3. *Typical set of curves of the discharge current as a function of the discharge voltage, at various pressures, with pure hydrogen. Magnetic induction, 1300 gauss. Anode length, 60 mm.; anode diameter, 20 mm.*

Fig. 3 shows a typical set of curves of the discharge current as a function of the discharge voltage at various pressures. The discharge tube was similar to that of Fig. 2 but with an anode cylinder 60 mm. in length and 20 mm. in inner diameter. These curves are similar to those of a cold cathode discharge between plane parallel electrodes in the absence of a magnetic field (35). The constant voltage curves correspond to the 'normal' discharge and the others to the 'abnormal' discharge. The part of the characteristics which occurs at currents of a few milliamperes is not shown. For the constant voltage characteristics, the ignition voltage was a few hundred volts higher than the voltage shown. With duralumin cathodes (AC17ST), the curves were similar but the minimum discharge voltage was about 350 v.

The discharge voltage varies with the state of the cathode surfaces. For the 4, 7, and 22 $\mu$ characteristic, the voltage can vary from 150 to 300 v., with magnesium. If the cathodes are well outgassed by operating the discharge at low pressure and high wattage without providing for heat dissipation, the minimum operating voltage may rise to 500 v. or more. It resumes its usual value of about 200 v. if the electrodes are exposed to air at a pressure of a few hundred microns for a few seconds. Thorough outgassing of the electrodes is thus not desirable. On the other hand, the discharge voltage was observed in many cases to decrease from an initial value of about 450 v. to about 250 v. after a few minutes of operation.

The 1 and 0.5 $\mu$ curves must be considered as qualitative; in this region, the characteristics cannot be reproduced satisfactorily. This can be attributed to the outgassing of the cathodes, which changes their electron emission properties. Outgassing also provides an erratic source of gas of uncertain composition.

Fig. 4 shows the discharge voltage and the discharge current at various pressures and magnetic fields. This curve shows the intersection of families of curves of the type of those of Fig. 3 with the resistance line, $L$. A supply voltage of 1500 v. and a series resistance of 20,000 ohms (including the internal resistance of the power supply) were used. The points corresponding to low pressures and high voltages must again be considered as qualitative.

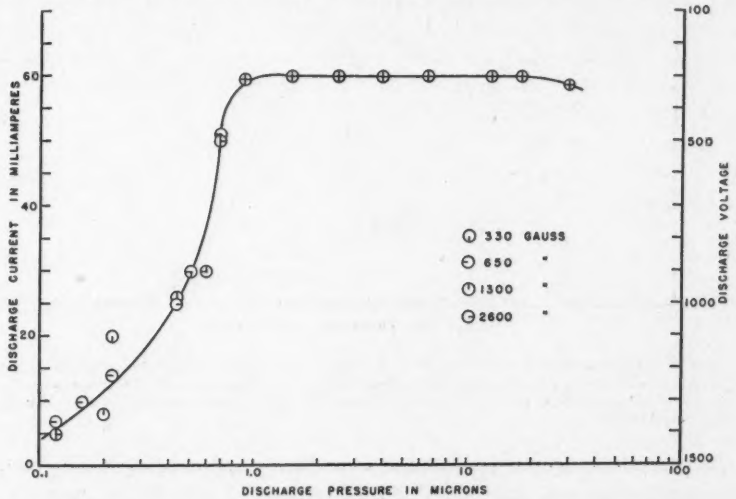



FIG. 4. *Discharge voltage and discharge current for various pressures and magnetic fields, with a mixture of 90% of hydrogen and 10% of oxygen collected over water. Power supply voltage, 1500 v.; series resistance, 20,000 ohms. Anode length, 26 mm.; anode diameter, 20 mm.*

Experience with many different discharge tubes of the same type and of the same order of size as the present ones has shown that the voltage–

pressure characteristic, as in Fig. 4, is determined mainly by the cathode material, and not by the geometry of the electrodes or by their spacing.

*2. Proton Production*

Figs. 5 and 6 show the percentage composition of the ion beam as a function of the pressure, with pure hydrogen, for anodes of two different sizes. The true discharge pressures for Fig. 5 are about the same as for Fig. 6; they are lower than the gauge pressures shown because of the small anode diameter used. The optimum proton content with pure hydrogen was about 10%. The percentage of $H^+_{3-1}$ and $H^+_{2-1}$ ions in the beam was of the order of 1%.

With electrolytic tank hydrogen, the beam composition was extremely variable, the proton content varying, for example, from 10 to 80% for apparently similar discharge conditions. The beam composition was especially variable at the beginning of a run when the discharge had not been operating for some time. No appreciable improvement was observed when the electrodes were water cooled. Similar inconsistencies have been observed by previous workers in this field (22). A set of curves of the percentage composition of the ion beam obtained under fairly steady conditions with electrolytic tank hydrogen was similar to those of Figs. 7 and 8 with a maximum proton content of 12%.

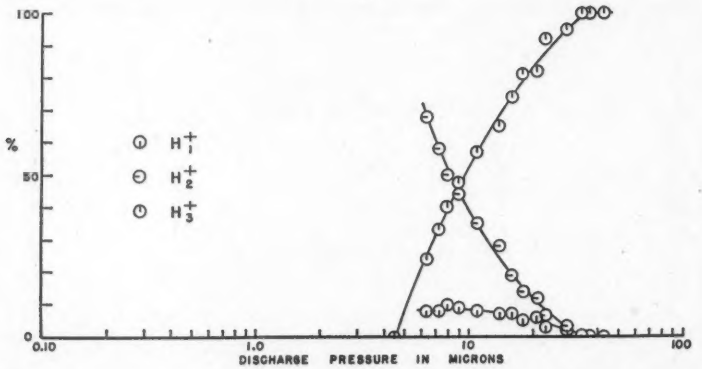



FIG. 5. *Percentage composition of the ion beam as a function of the pressure, with pure hydrogen. The gauge pressures shown are higher than the true pressures by a factor of about 3. Magnetic induction, 780 gauss; discharge current, 30 ma. Anode length, 26 mm.; anode diameter, 13 mm.*

The very high proton percentages were highly encouraging, even though erratic. It appeared that the 0.3% of oxygen present in the electrolytic hydrogen reduced the recombination of atomic hydrogen at the walls of the discharge tube and thus provided a higher concentration of atomic hydrogen (see below).

Various poisons were added to the electrolytic hydrogen in the hope of obtaining a reliable high proton percentage in the ion beam. Air, water

vapor, and hydrogen chloride vapor had no appreciable effect. The hydrogen chloride vapor was added by bubbling the hydrogen in concentrated hydrochloric acid at 0° C.

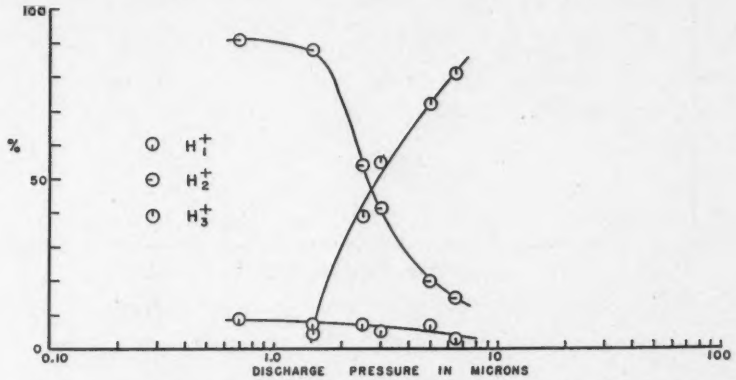



FIG. 6. *Percentage composition of the ion beam as a function of the pressure, with pure hydrogen. Magnetic induction, 780 gauss; discharge current, 30 ma. Anode length, 60 mm.; anode diameter, 20 mm.*

The addition of oxygen produced a definite improvement. For given discharge conditions, the proton percentage in the ion beam increased until the gas contained 10% of oxygen. Further addition of oxygen had little effect. Fig. 7 shows the ion beam composition for the same discharge tube as that of

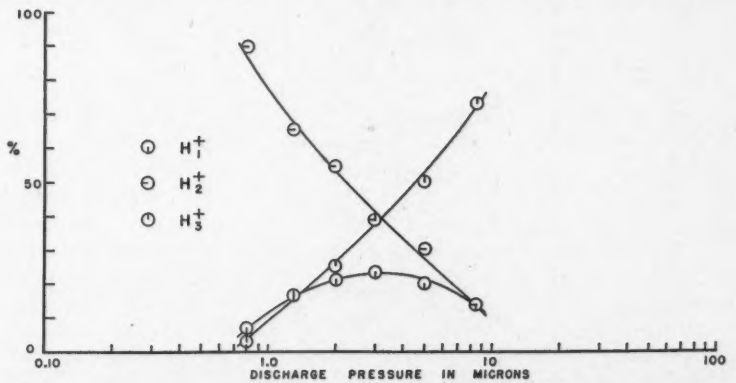



FIG. 7. *Percentage composition of the ion beam as a function of the pressure, with a mixture of 90% of hydrogen and 10% of oxygen collected over water. Magnetic induction, 780 gauss; discharge current, 30 ma. Anode length, 60 mm.; anode diameter, 20 mm.*

Fig. 6 and for the same operating conditions, but with a mixture of 90% of electrolytic tank hydrogen and 10% of tank oxygen collected over water at room temperature. Fig. 8 shows a similar set of curves for a shorter anode.

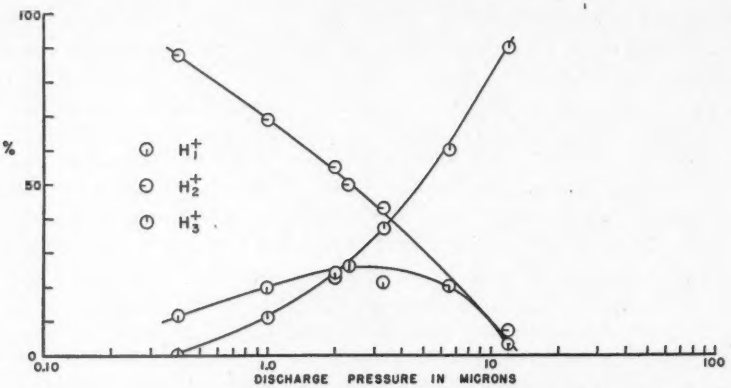



FIG. 8. *Percentage composition of the ion beam as a function of the pressure, with a mixture of 90% of hydrogen and 10% of oxygen collected over water. Magnetic induction, 780 gauss; discharge current, 30 ma. Anode length, 26 mm.; anode diameter, 20 mm.*

The percentage of oxygen and other foreign ions in the beam was only about 1%. It is to be noted that the increase in the proton percentage was *not* accompanied by a corresponding decrease in the total ion current.

Fig. 9 shows the percentage composition of the ion beam for the same discharge tube and for the same gas mixture as for Fig. 8, at a pressure of 2 $\mu$, for various discharge currents and magnetic fields.

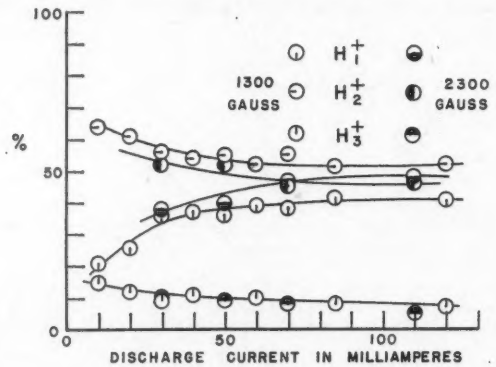



FIG. 9. *Percentage composition of the ion beam as a function of the discharge current, with a mixture of 90% of hydrogen and 10% of oxygen collected over water. Discharge pressure, 2 $\mu$. Anode length, 26 mm., anode diameter, 20 mm.*

Fig. 10 shows the variation in the ion beam composition at a discharge current of 30 ma., as the magnetic field is increased from 400 to 3200 gauss.

When the ion beam is extracted from the edge of the cathode, its composition is about the same as when it is extracted from the centre, as in Fig. 2.

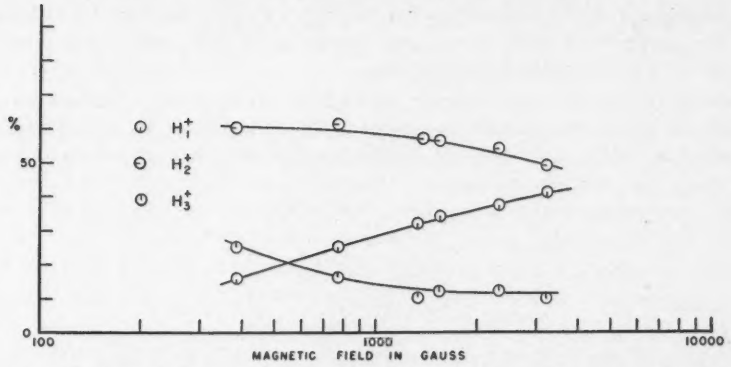



FIG. 10. *Percentage composition of the ion beam as a function of the magnetic field at the discharge, with a mixture of 90% of hydrogen and 10% of oxygen collected over water. Discharge pressure, 2 μ; discharge current, 30 ma. Anode length, 26 mm.; anode diameter, 20 mm.*

### *3. Ionization Processes*

The probable ionization and dissociation processes in hydrogen are as follows (3, 9, 16, 18, 27, 29, 36, 37, 38).

$$H_2 + e \rightarrow H_2^+ + 2e \qquad (A)$$
$$\rightarrow H_1 + H_1 + e \qquad (B)$$
$$\rightarrow H_1^+ + H_1 + 2e \qquad (C)$$
$$H_2^+ + H_2 \rightarrow H_1^+ + H_1 + H_2 \qquad (D)$$
$$\rightarrow H_3^+ + H_1 \qquad (E)$$
$$H_3^+ + H_2 \rightarrow H_1^+ + 2H_2 \qquad (F)$$
$$H_1 + e \rightarrow H_1^+ + 2e \qquad (G)$$

The ionization potentials for (*A*) and (*C*) are about 17 v. (3, 4, 38). Molecular ions from (*A*) have energies of a few electron volts, while atomic ions from (*C*) have thermal energies (29). The cross section for (*A*) is a maximum for electrons of about 75 v. and is about 200 times that for (*C*) (29). Process (*C*) thus probably has little importance for a proton source. Reaction (*B*) has been investigated both experimentally (9, 18) and theoretically (27). Its cross section is particularly high for 15 volt electrons, about 6 times the maximum cross section for Reaction (*A*). Reactions (*D*) and (*F*) are observed in mass spectrographs when accelerated $H_2^+$ and $H_3^+$ ions collide with neutral molecules before entering the magnetic field, giving rise to ions whose apparent mass is $\frac{1}{2}$ or $\frac{1}{3}$ of that of a proton, usually designated as $H_{2-1}^+$ or $H_{3-1}^+$ (16, 37).

Glass and metallic surfaces catalyze the recombination of atomic hydrogen to molecular hydrogen, but glass can be poisoned by mixing oxygen or water vapor with the hydrogen or by coating it with metaphosphoric acid. Tungsten surfaces can be poisoned with oxygen (43). The absence of dust and of organic matter is important, and the surfaces should preferably be

cool to reduce the recombination (11, 39, 43). Under optimum conditions, a hydrogen discharge tube operating at a pressure of 200 to 500 $\mu$ can contain 20 to 50% of atomic hydrogen (39, 43).

In Figs. 5 and 6, the curves for $H_2^+$ and $H_3^+$ show the high probability of Reaction (*E*): as the pressure is increased, the percentage of $H_2^+$ ions decreases while that of $H_3^+$ ions increases until the beam is composed almost exclusively of $H_3^+$. The $H_3^+$ ions appear to be formed mainly through Reaction (*E*). The competing reaction (*D*) cannot thus be the main source of atomic ions, since the $H_1^+$ and $H_3^+$ curves are entirely different in shape. The 8% of atomic ions which is found at the lower pressures when the percentage of $H_3^+$ is negligible cannot be attributed to (*F*). Also, from the fact that the percentage of $H_3^+$ rises to 100 at the higher pressures, it must be inferred that Reaction (*F*) is quite rare in the present discharge. Then the atomic ions must originate mainly from (*G*). The atomic hydrogen required can be produced either through (*B*) or through (*E*). The latter reaction obviously contributes very little to the formation of atomic ions here, since the percentage of $H_1^+$ decreases as that of $H_3^+$ increases.

By a process of elimination, one is thus led to believe that, in the present source, the atomic ions are formed mainly through (*B*) and (*G*):

$$H_2 + e \rightarrow H_1 + H_1 + e \qquad (B)$$

$$H_1 + e \rightarrow H_1^+ + 2e \qquad (G)$$

The importance of these two reactions is confirmed by the fact that much higher percentages of atomic ions are found when the walls of the discharge tube are poisoned to reduce the rate of recombination of atomic hydrogen and thus increase its concentration in the gas.

The results of other workers in this field hardly agree with each other and with the present results. This can be attributed to differences in the energy distribution of the ionizing electrons, and in the discharge tube surfaces.

H. D. Smyth's results on the primary and secondary products of ionization in hydrogen (37), when plotted as in Figs. 5 and 6 give for the ion $H_2^+$ a curve that is entirely similar to the present ones, but his curve for $H_3^+$ shows no discontinuity at the low pressures, and his maximum percentage of $H_3^+$ is only about 80. He observed an *increase* in the percentage of atomic ions with pressure and attributed their formation to Reaction (*D*).

L. P. Smith and G. W. Scott (34, 36) have reported a proton source for which the atomic ion percentage *decreased* sharply with pressure. These authors explain the formation of atomic hydrogen in their source by Reactions (*B*) and (*G*) at low pressures and also by (*C*) and by (*A*), (*E*), and (*G*). They do not give data on the $H_2^+$ and $H_3^+$ ions.

O. Luhr (26) has observed that hydrogen ions aged to $10^5$ collisions in hydrogen at a pressure of 300$\mu$ contain 10% of $H_1^+$, 10% of $H_2^+$, and 80% of $H_3^+$. This is not in agreement with the present results nor with H. D. Smyth's curves.

The marked increase in the proton percentage that occurs upon the addition of oxygen and of water vapor to the hydrogen (Figs. 7 and 8) is presumably due to a decrease in the rate of recombination of atomic hydrogen at the walls of the discharge tube. At the lower pressures, the metal surfaces are probably outgassed so that the surfaces favor the recombination of atomic hydrogen as if the oxygen and the water vapor were not present.

The curves of Figs. 9 and 10, showing the composition of the ion beam as a function of the discharge current and of the magnetic field, can be explained qualitatively. The rate of production of atomic hydrogen should increase with the density of the slow electrons available for dissociation in the discharge tube, and thus with the discharge current. When the magnetic field is increased at constant discharge current, the rate of drift of the electrons toward the anode is reduced and the density of slow electrons increases. Then, increasing either the discharge current or the magnetic field should (*a*) increase the percentage of atomic ions; (*b*) reduce the percentages of both the $H_2^+$ and $H_3^+$ ions, if these are formed according to Equations (*A*) and (*E*); (*c*) reduce the ratio of the percentage of $H_3^+$ to the percentage of $H_2^+$ if the $H_3^+$ ions are formed according to Equation (*E*).

*4. Ion Extraction*

A positive ion beam can be extracted from a gas discharge either in the form of a canal ray through a hole in the cathode or directly from the discharge plasma. Figs. 11 (*a*) and 11 (*b*) show schematically these two types of extraction with the present type of discharge. Fig. 11 (*c*) is a proposed modification of Fig. 11 (*b*) for the cyclotron. The first two types were investigated very briefly. Unfortunately, time did not allow a more thorough

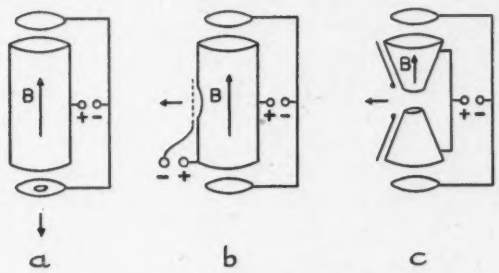



FIG. 11. *The extraction of the ion beam.*

investigation of the ion extraction. No attempt was made to obtain large ion beam currents. The results obtained, however, will indicate orders of magnitude, if not optimum conditions.

For the former case, discharge tubes similar to that shown in Fig. 2 and varying only as to the dimensions of the anode cylinder, were used. The hole in $K_2$ had a diameter of 2 mm. and its area was 2% of that part of the cathodes

that projects in the anode cylinder. Under these conditions, the ratio of the total ion beam current (including secondary electrons from the target) to the discharge current varied from 2 to 1% as the discharge current was increased from 10 to 100 ma. The dimensions of the anode had but little effect on this ratio. The pressure also had little effect, as long as the discharge was operated in the constant voltage region.

A small hole was used in $K_2$ so as to maintain a low pressure in the mass spectrograph. A somewhat larger hole would presumably have given a higher ratio of ion beam current to discharge current.

The extraction was much more efficient at low pressures and high discharge voltages. In one case, for instance, the ratio of the ion beam current to the discharge current was 1.3% when the discharge was operated at 300 v., while it was 16% at 1000 v. Unfortunately, this high efficiency of extraction cannot be utilized, as it is accompanied by a relatively low efficiency of proton production.

An ion beam can also be extracted from the discharge plasma through a side hole in the anode cylinder by means of a grid maintained at a negative potential with respect to the anode, as in Fig. 11*b*. In the one source of this type that was built, the anode cylinder was 25 mm. long and 13 mm. in diameter, and was drilled with a side hole 6 mm. in diameter. The grid was at a distance of a few millimetres from the hole and its transparency was roughly 25 or 50%. The ion beam current increased as the grid was made more negative with respect to the anode, until the extracting potential was about 500 v. A further increase in the extracting potential had little effect on the ion beam current.

Under these conditions, the ratio of the ion beam current (including the current to the grid and secondary electrons from the target) to the discharge current was about 10%. The grid intercepted most of the ions, but with a proper design, the current to the extracting electrode could probably be less than one-half of the total ion current. The effective ratio of the ion beam current (including secondary electrons) to the total discharge current can thus be taken as 5% for the above discharge tube.

The ratio of the number of protons to the number of unionized particles emitted by the source can be calculated approximately as follows. Let

$N_u$ = Number of unionized particles emitted by the source per second;
$N_i$ = Number of ionized particles emitted per second;
$N_p$ = Number of protons emitted per second;
$i_m$ = Measured ion beam current, in milliamperes;
$i$ = True ion beam current in milliamperes;
$d$ = Diameter of the orifice through which the ion beam is extracted;
$p$ = Pressure in the discharge tube, in microns;
$M$ = Average molecular weight of the gas used.

Then

$$N_i = 6.3 \times 10^{15}\, i\,. \qquad (H)$$

Assuming that the pressure in the discharge tube is much higher than that in the mass spectrograph (or in the ion accelerator),

$$N_u = 1.3 \times 10^{16} \frac{d^2 p}{\sqrt{M}} . \qquad (I)$$

The gas mixture (composed of about 90% of hydrogen, 10% of oxygen, and 2% of water vapor) which was used, had an average molecular weight of about 4, assuming that 50% of the hydrogen in the discharge tube was in the atomic state. We thus have

$$\frac{N_i}{N_u} = \frac{i}{d^2 p} . \qquad (J)$$

In the present case, the measured ion beam current $i_m$ included the secondary electron current; a rough correction for this can be made by writing $i = i_m/1.5$. Then, since about 50% of the ions formed were protons, under optimum conditions,

$$\frac{N_p}{N_u} = \frac{i_m}{3d^2 p} . \qquad (K)$$

For the case of endwise extraction through one of the cathodes, we had, in one case, $i_m = 1$ ma., $d = 2$ mm., and $p = 2\mu$, and

$$\frac{N_p}{N_u} = 4\% . \qquad (L)$$

This is not a maximum value; higher values of $N_p/N_u$ could be obtained by using a higher discharge current. A change in the size of the orifice in the cathode at constant discharge current would not produce a large change in this ratio, since $N_i$ and $N_p$ are proportional to the area of the orifice, like $N_u$, at least to a first approximation.

With sidewise extraction through a hole in the anode cylinder, the discharge currents used were low, about 10 ma. and the resulting value of $N_p/N_u$ was about one-tenth of the above value. The ion beam current per unit area of the extraction hole and per unit discharge current was about 2.5 times lower for sidewise extraction than for endwise extraction.

The ratio of the proton current $i_p$, in microamperes, in the ion beam, to the wattage, $W_d$, dissipated in the discharge for endwise extraction, with 250 v. and 100 ma. at the discharge, and 1 ma. in the ion beam, was 13 $\mu$a. per watt. Again, this is not the maximum value; higher values could be obtained by using a larger extraction hole.

For sidewise extraction, with 250 v. and 10 ma. at the discharge, and 0.5 ma. in the ion beam, the above ratio was 67 $\mu$a. per watt. This is probably about the optimum value for sidewise extraction. The dissipation of the heat developed in the source for either type of extraction presents no serious problem.

The energy of the extracted ions, for endwise extraction, is given approximately by the discharge voltage. The energy spread was low, as could be judged by the sharpness of the maxima of the mass spectrum, less than 1% of

the mean energy, i.e., less than about 2 v. When the discharge was operated at high voltages, the energy spread was very much larger and increased with the discharge voltage.

The intensity of the ion beam current can be varied, for both types of extraction, by varying the discharge current with a rheostat in series with the discharge.

An electron beam can be extracted from the discharge by applying a positive potential on the cylinder $L$ (Fig. 2). The electrons give a much more luminous beam than the positive ions because of their higher efficiency for excitation and ionization (6). A fine sharp beam was obtained with an accelerating potential of only 20 v. on $L$, indicating that the energy of the electrons as they emerged from $K_2$ was very low. M. von Ardenne has designed a source that can supply either a positive ion or an electron beam, for use with a Van de Graaff accelerator (2).

The ion source shown in Fig. 2 was designed purely for the purpose of investigating its discharge characteristics and its mass spectrum. It would not be convenient as an ion source for an accelerator.* In designing such a source, a choice will have to be made between endwise and sidewise extraction of the ion beam. The latter type of extraction has the distinct advantage that it permits the use of the high magnetic field of a C-type permanent magnet. A mass analysis of the ion beam could probably be made in the field of a second C-type magnet near the discharge tube where the ion beam has an energy of only a few hundred volts. M. von Ardenne has described a mass monochromator which could be used with either type of extraction (1).

With endwise extraction, it seems that the magnetic field for the discharge would have to be provided by one or two coils, as in Fig. 2. A tubular permanent magnet surrounding the discharge tube could also be used (42), but then the magnetic induction would only be a few hundred gauss and the optimum proton percentage probably about 20%.

The discharge tube should present only magnesium, brass, and glass surfaces to the gas, since it is doubtful that many other surfaces are poisoned by oxygen and water vapor in the manner described above (43).

A deuteron source would not require a higher magnetic field than a proton source, since the main action of the magnetic field is on the electrons.

## Conclusions

The ion source described above possesses to a satisfactory degree the desirable characteristics enumerated in the Introduction.

The table shown below will serve to compare the present source with the various other types. In cases where a number of papers have been published on the same type of source, reference is made to the most recent one. The figures shown are necessarily approximate, since the operating conditions can vary; they have been chosen to represent the average characteristics.

** A further paper will be published shortly describing an ion source of the present type for use with a linear accelerator and providing a high ion beam current.*

TABLE I

APPROXIMATE CHARACTERISTICS OF VARIOUS TYPES OF POSITIVE ION SOURCE

| Type | Year | Filament | Energy spread, v. | $i$, ma. | $\frac{i_p}{i}$, % | $\frac{i_p}{W_d}$, μa./w. | $\frac{N_p}{N_u}$, % |
|---|---|---|---|---|---|---|---|
| Low-pressure glow-discharge (Penning) (32) | 1937 | No | 10,000 | 0.5 | Very low[1] | Very low[1] | Very low[1] |
| Palladium tube (14, 15) | 1938 | | 0.2 | 0.2 | ? | ? | $10^{-4}$ |
| Electron beam (36) | 1939 | Yes | 500 | 1 | 60 | 3 | 6 |
| Low-pressure arc (Finkelstein) (12) | 1940 | Yes | <2[1] | 150 | ? | ? | ? |
| Pyrex capillary (22) | 1941 | Yes | 30 | 1.5 | 60 | 6.7 | 3.6 |
| Canal ray tube (7) | 1942 | No | 25,000 | 1.5 | 45 | 1 | 0.2 |
| Low-pressure arc (von Ardenne ) (1, 2) | 1943 | Yes | <2[1] | 0.1 | 50 | 5 | 0.4 |
| High-frequency discharge (40) | 1946 | No | 20,000 | 0.3 | ? | ? | ? |
| Cyclotron (23) | 1946 | Yes | 50 | 100[1] | 10[1] | 5.6[1] | 4[1] |
| Low-pressure glow-discharge (present work) | 1947 | No | <2 | 1 | 50 | 67 | 4 |

[1] *Probable value.*

## Acknowledgments

The writer wishes to express his thanks to Dr. J. S. Foster and to Dr. B. W. Sargent for suggesting the problem, and to Mr. A. G. Ward for his valuable advice in the first few months of this work. The writer also wishes to express his indebtedness to the National Research Council of Canada for the award of a Grant for Research which greatly facilitated the progress of the work.

## References

1. ARDENNE, M. v. Physik. Z. 43 : 91-101. 1942.
2. ARDENNE, M. v. Z. Physik, 121 : 236-267. 1943.
3. BLEAKNEY, W. Phys. Rev. 35 : 1180-1186. 1930.
4. BRODE, R. B. Rev. Modern Phys. 5 : 257-279. 1933.
5. BURCHAM, W. E. Unpublished report MP-176. The development of a source of fast neutrons of variable energy. National Research Council of Canada. 1945.
6. COBINE, J. D. Gaseous conductors; theory and engineering applications. McGraw-Hill Book Co., Inc., New York. 1941.
7. CRAGGS, J. D. Proc. Phys. Soc., London, 54 : 245-265. 1942.
8. DEMPSTER, A. J. Phys. Rev. 11 : 316-325. 1918.
9. DORSCH, K. E. and KALLMANN, H. Z. Physik, 53 : 80-91. 1929.
10. DRUYVESTEYN, M. J. and PENNING, F. M. Rev. Modern Phys. 12 : 87-174. 1940.
11. FARKAS, A. and MELVILLE, H. W. Experimental methods in gas reactions. Macmillan & Co., Ltd., London. 1939.
12. FINKELSTEIN, A. T. Rev. Sci. Instruments, 11 : 94-97. 1940.
13. FOWLER, R. D. and GIBSON, G. E. Phys. Rev. 46 : 1075-1086. 1934.

14. FRANZINI, T. Nuovo cimento, 15 : 88-99. 1938.
15. FRANZINI, T. Atti accad. Lincei, 27 : 292-297. 1938.
16. FRIEDLÄNDER, E., KALLMANN, H., LASAREFF, W., and ROSEN, B. Z. Physik, 76 : 60-69. 1932.
17. HEIL, H. Z. Physik. 120 : 212-226. 1942.
18. HUGHES, A. LL. and SKELLETT, A. M. Phys. Rev. 30 : 11-25. 1927.
19. HULUBEI, H. Compt. rend. 199 : 199-201. 1934.
20. JOSSEM, E. L. Rev. Sci. Instruments, 11 : 164-166. 1940.
21. KORSCHING, H. Physik. Z. 42 : 74-79. 1941.
22. LAMAR, E. S., BUECHNER, W. W., and VAN DE GRAAFF, R. J. J. Applied Phys. 12 : 132-140. 1941.
23. LIVINGSTON, M. S. Rev. Modern Phys. 18 : 293-299. 1946.
24. LIVINGSTON, M. S., HOLLOWAY, M. G., and BAKER, C. P. Rev. Sci. Instruments, 10 : 63-67. 1939.
25. LORRAIN, P. Unpublished report PD-158. A cold cathode discharge for use in an ion source. National Research Council of Canada. 1945.
26. LUHR, O. Phys. Rev. 44 : 459-462. 1933.
27. MASSEY, H. S. W. and MOHR, C. B. O. Proc. Roy. Soc., London, A135 : 258-275. 1932.
28. MAXWELL, L. R. Rev. Sci. Instruments, 2 : 129-140. 1931.
29. NEWHALL, H. F. Phys. Rev. 62 : 11-18. 1942.
30. PENNING, F. M. Physica III : 873-894. 1936.
31. PENNING, F. M. Physica IV : 71-75. 1937.
32. PENNING, F. M. and MOUBIS, J. H. A. Physica IV : 1190-1199. 1937.
33. RITSCHL, R. Physik. Z. 38 : 141-157. 1937.
34. SCOTT, G. W., JR. Phys. Rev. 55 : 954-959. 1939.
35. SEELIGER, R. Einführung in die Physik der Gasentladungen. J. A. Barth, Leipzig. 1927.
36. SMITH, L. P. and SCOTT, G. W., JR. Phys. Rev. 55 : 946-953. 1939.
37. SMYTH, H. D. Phys. Rev. 25 : 452-468. 1925.
38. SMYTH, H. D. Rev. Modern Phys. 3 : 347-391. 1931.
39. STEACIE, E. W. R. Atomic and free radical reactions; the kinetics of gas phase reactions involving atoms and organic radicals. Reinhold Publishing Corporation, New York. 1946.
40. THONEMANN, P. C. Nature, 158 : 61. 1946.
41. WALCHER, W. Z. Physik, 122 : 62-85. 1944.
42. WARD, A. G. Unpublished report PM-148. Notes on positive ion sources. National Research Council of Canada. 1945.
43. WOOD, R. W. Proc. Roy. Soc., London, A102 : 1-9. 1922.

# THERMAL CONDUCTIVITY OF METALS AT HIGH TEMPERATURES[1]

## I. DESCRIPTION OF THE APPARATUS AND MEASUREMENTS ON IRON

By L. D. Armstrong[2] and T. M. Dauphinee[2]


## Abstract

An apparatus for measuring the thermal conductivity of metals in the temperature range 0° to 800° C. is described. The method utilizes unidirectional heat flow in a cylindrical sample in a vacuum. The advantages of the method are outlined and a comprehensive analysis of possible errors in the measurements is included. Measurements on Armco iron indicate that results with an absolute error of less than 2% may be obtained. The results of measurements on a sample of Armco iron gave thermal conductivities of 0.181, c.g.s. units at 0° C. and 0.069, c.g.s. units at 800° C. A change in slope of the thermal conductivity – temperature curve was found at a temperature of approximately 375° C., and is tentatively attributed to the presence of 0.03% nickel impurity.


## Description of the Apparatus

### *Introduction*

The thermal conductivity of metals at high temperatures has considerable theoretical and practical interest. It provides a valuable check on the theories of the solid state, which are still in a condition of considerable uncertainty. Its practical value is well demonstrated by the demand for thermal conductivity data that has arisen as a result of recent developments in nuclear physics and jet propulsion. For these and other reasons, additional information on thermal conductivities would be very valuable.

An apparatus for the measurement of thermal conductivity at high temperatures should be adaptable to the measurement of conductivities of a large number of metals and it should operate over as wide a temperature range as possible. Since some metals are very active chemically, a vacuum apparatus is desirable. Moreover, some metals are not available in large quantities and consequently the apparatus should use the smallest samples with which accurate results can be obtained. The presence of transition points and the non-linearity of the thermal conductivity – temperature relation necessitate the use of small temperature intervals.

### *Method of the Experiment*

The measurement of the temperature, heat flow, and dimensions is complicated by a number of factors. As the temperature interval must be measured between points in a temperature gradient, thermocouples are generally required instead of the more sensitive resistance thermometers. This limits the accuracy with which the small temperature intervals can be measured. In general, it is not feasible to measure the heat flow in the same

[1] *Manuscript received in original form June 7, 1947, and, as revised, August 27, 1947.*
*Contribution from the Division of Physics and Electrical Engineering, National Research Laboratories, Ottawa, Canada. Issued as N.R.C. No. 1620.*

[2] *Physicist.*

region as the temperature gradient. Consequently, precautions have to be taken to prevent undesirable heat exchanges from radiation and conduction. Many other considerations arising from the criteria previously outlined must be taken into account.

The method selected is one using axial, unidirectional heat flow in a cylindrical sample, between a measurable heat source and a heat sink, with appropriate shielding to prevent errors due to radiation and conduction. The temperature gradient is measured by thermocouples peened into the sample a known distance apart, and the entire unit is operated in a vacuum. The thermal conductivity is then calculated using the formula:

$$K_T = \frac{Q \times L}{A\,(T_2 - T_1)}, \tag{1}$$

where $K_T$ = thermal conductivity in calories per square centimetre per second for a temperature gradient of 1° C. per centimetre at temperature $T$ ° C.,

$Q$ = heat input in calories per second,

$L$ = separation of measuring thermocouples in centimetres,

$A$ = cross sectional area of sample in square centimetres,

$T_2 - T_1$ = temperature interval in ° C.,

$$T = \frac{T_2 + T_1}{2}.$$

*Apparatus*

A cross sectional view of the apparatus is shown in Fig. 1. The sample, *A*, is a solid cylinder 8.00 cm. long and 2.50 cm. in diameter, and rests on the centre portion of the heat sink, *B*. The sample heater element (10 w.) is a helix of platinum – 10% rhodium wire cemented in grooves in the sample heater, *C*. The sample cap, *D*, covers the exposed sides of the sample heater. The guard sleeve, *E*, is a cylindrical iron tube concentric with the sample and, like it, resting on the heat sink. It has two heating coils of platinum–rhodium wire, one at the top and the other near the bottom. The guard cap, *F*, supported by ceramic insulators on the guard sleeve, surrounds the exposed sides of the sample cap. The guard cap has a heating element of platinum–rhodium wire in grooves on the top. The heat sink, *B*, is a machined gold block, with a non-inductive heating coil wound in ceramic cement in the lower portion. It is securely attached to the supporting column, *G*, by a cone joint and screw.

The supporting column is a thin walled iron tube that passes through the bottom of the 'pyrostat'.* Its upper section contains a spiral coil through which air or water may be circulated. The pyrostat encloses the main part of the apparatus and may be maintained at the desired temperature by the furnace, *H*, while cooling coils prevent the ends from overheating. The

** The authors have been unable to find any simple term to represent the container that surrounds the apparatus. Since this container performs the same function at high temperatures as a cryostat does at low temperatures it has been given the name of 'pyrostat'.*

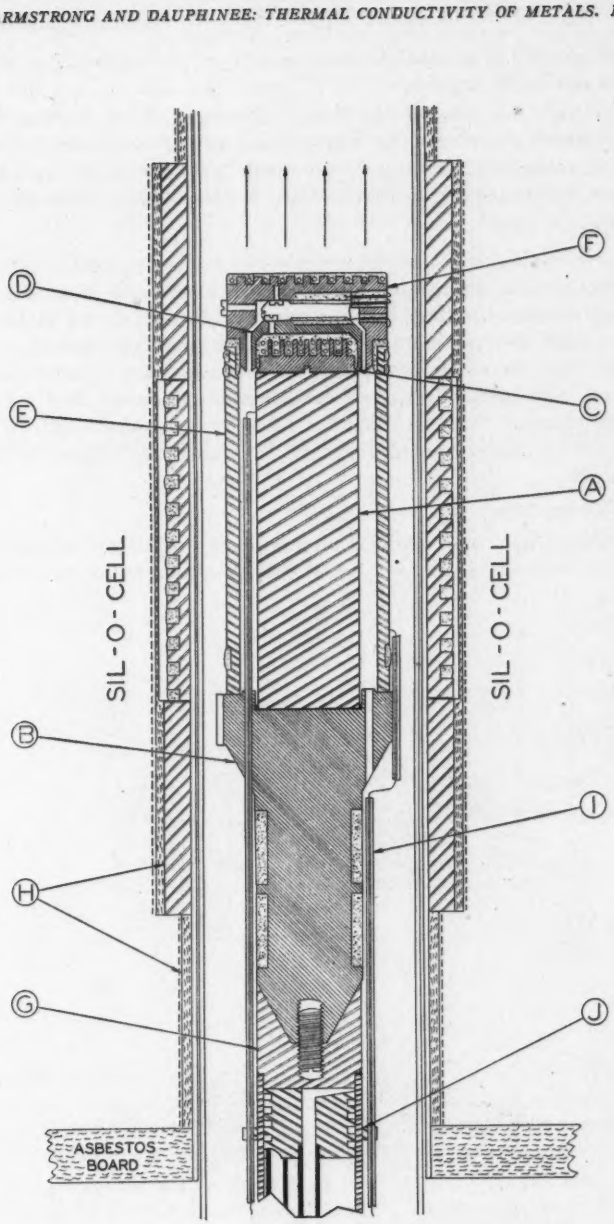



FIG. 1.

vacuum connections are made at the top of the pyrostat and the lead wires are taken out at the bottom.

All lead wires are taken to the base of the apparatus in fine bore ceramic tubing, *I*, which acts both as an insulator and as a rigid support. Above the supporting column this tubing is fitted into holes drilled in the heat sink, while along the supporting column it is held in slotted collars, *J*, by spring clips.

*The Furnace*

The furnace, *H* (Fig. 1), which fits loosely over the pyrostat, consists of a five section winding on a stainless steel tube. In order to provide a uniform temperature region the three centre sections are wound over $\frac{1}{4}$ in. thick steel sleeves. A 200 ohm platinum resistance thermometer is embedded in a spiral groove cut into the centre sleeve, and thermocouples are installed under the winding of each section. The outer wall is a galvanized iron cylinder on which are mounted terminal strips for the electrical connections. The ends are closed with asbestos board disks and the furnace is insulated with diatomaceous silica.

*Vacuum Connections*

The vacuum line to an oil diffusion pump is joined to the apparatus by a faced metal-to-metal seal. A sylphon bellows allows for thermal expansion

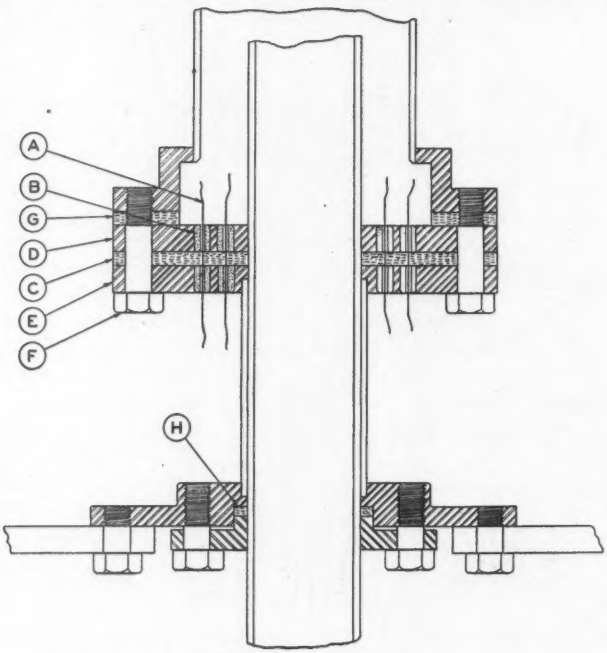



FIG. 2. *Vacuum seal.*

of the pyrostat. The bottom of the pyrostat is sealed with rubber gaskets as shown in Fig. 2. The lead wires, *A*, are threaded through the insulating beads, *B*, and the rubber gasket, *C*. The beads are set into the steel plates, *D*, *E*, which are clamped together by means of screws, *F*, compressing the rubber and making an effective vacuum seal. Other rubber gaskets, *G*, *H*, are used to seal the centre column and the pyrostat tube. This assembly has functioned very satisfactorily and no difficulty has been encountered in maintaining pressures of less than 1 $\mu$.

*Power Circuits*

The power for the sample, guard sleeve, and guard cap heaters is taken from a common source regulated to maintain voltage constant to 0.1%. The circuits may be adjusted simultaneously by controlling this source, or independently by rheostats in the individual circuits (Fig. 3). To prevent

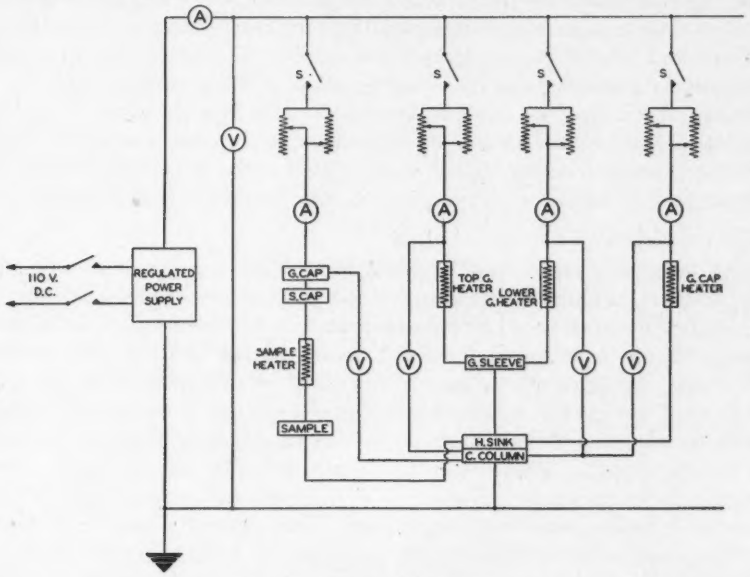



FIG. 3. *Heater control circuits.*

heat conduction errors, current and potential leads are not attached directly to the sample heater element. The connections are made to the guard cap. Short wires connect the guard cap to the sample cap and the sample cap to the heater element. The centre column serves as ground. Since the guard cap is part of the sample heater circuit, the ground lead for the guard cap heater element is connected to the heat sink. The sample heater current and voltage are shown by accurate meters calibrated to 1/10% full scale, while large panel meters are used for all other circuits.

The sink heater is fed from the 110 v. d-c. mains through a rheostat control with fine and coarse adjustment. A reversing relay is connected in this circuit to check for magnetic effects due to the heater.

The furnace wiring circuit is shown in Fig. 4. Power is supplied from the 110 v. a-c. mains and controlled by means of a 5 kva. variable voltage transformer. A saturable reactor in series provides fine control, and may, if desired, be used in conjunction with the resistance thermometer for automatic temperature regulation. Uniform furnace temperatures can be established by adjusting the variable transformers in series with each of the five sections of the winding.

*Thermal Contacts*

In Equation (1) it is assumed that rectilinear heat flow exists throughout the region in which the temperatures are measured. For this to be true in regions close to an interface it is essential that the heat flow across the interface be uniform. One of the simplest ways of securing this uniformity is to reduce the thermal resistance to a minimum by means of a low melting point intermediate metal that will 'wet' both surfaces. Tin is satisfactory for many materials and has been used in the preliminary measurements on Armco iron. At the conclusion of the tests it was found that the joints had become so strong that they could be broken only with difficulty even at high temperatures.

*The Use of Gold*

An interesting point came up during the preliminary experiments on the apparatus. At that time the heat sink was made of copper, and it was found that after the apparatus had been evacuated and maintained at 500° C. for some time the regions around the sink became coated with a reddish deposit of copper, owing to the formation of unstable volatile hydrides or nitrides. The small amounts of hydrogen and nitrogen present in the pyrostat react with the copper, and the compounds formed subsequently dissociate to leave a metallic deposit. Since evaporated copper on the fine thermocouples in the apparatus might easily cause errors in temperature measurement, it was advisable to eliminate such evaporation. Investigation showed that many other metals behave similarly at high temperatures. Gold appeared to be the only metal having the desired characteristics, namely, small evaporation under working conditions, relatively high thermal conductivity, and a melting point well above 900° C. Consequently, gold was used for all parts of the apparatus requiring these characteristics; namely, for the sample heater, sample cap, guard cap, and heat sink.

Observations at the conclusion of the first series of experiments showed that some evaporation of the gold had taken place. In addition, any excess of tin around the edges of the contacts had spread over the neighboring surfaces of the gold, forming a low melting point alloy which crystallized on subsequent cooling.

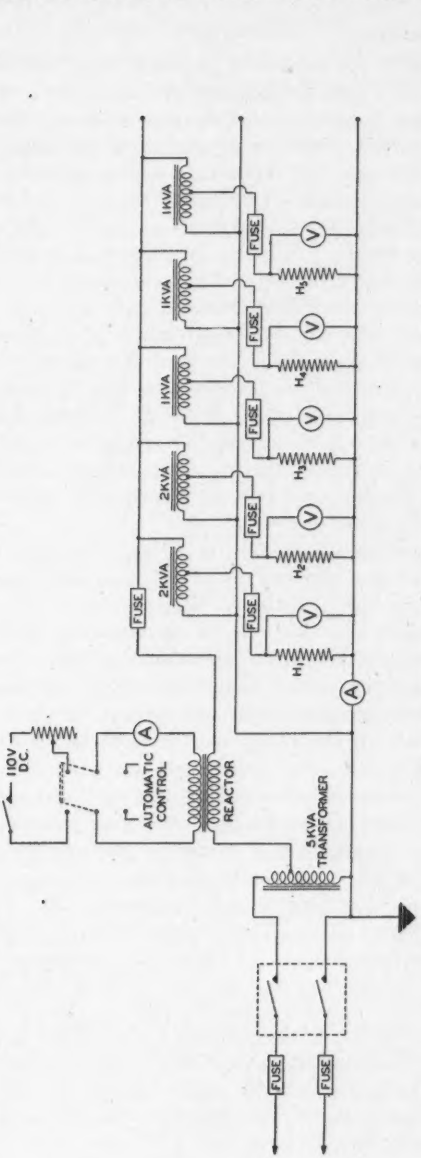



FIG. 4. *Furnace control circuit.*

*Temperature Measurement*

Except for the use of the resistance thermometer in the furnace, temperatures are measured by means of platinum–platinum–rhodium thermocouples. The sample, guard sleeve, and heat sink thermocouples are attached by making a shallow and very narrow groove on the surface of the metal perpendicular to the axis, and, after laying in the thermocouple, peening down the sides of the groove until the thermocouple is completely enclosed and wedged in place. The sample thermocouples are spaced approximately 5 cm. apart, the upper one being 1 cm. from the top. Since the position of these thermocouples must be known very accurately, 0.003 in. wire and very small butt-welded junctions (1) are used; the separation of the thermocouples is measured with a travelling microscope. Similar thermocouples are attached to the outside of the guard sleeve opposite those on the sample. In order that no heat will be conducted along the wires to the junction, the leads of these four thermocouples are taken halfway around the sample or guard sleeve at the same level before being taken to the base of the apparatus. Fine wire thermocouples are embedded in ceramic cement in grooves on the top of the sample cap and the underside of the guard cap. The leads are brought out through holes in the guard cap and down outside the guard sleeve.

Two thermocouples are mounted in the air space between the guard sleeve and the pyrostat wall, one near the top of the guard sleeve and the other near the bottom, to give an indication of the temperature gradient in the pyrostat. The five thermocouples mentioned in the description of the furnace are used to determine the temperatures and gradients in the furnace itself. Since their response to changes in the furnace heating current is considerably more rapid than that of the thermocouples inside the pyrostat, these thermocouples are used in conjunction with the resistance thermometer in the control of the furnace temperature.

The leads of all thermocouples are taken to a felt insulated metal zone box where they are connected to copper lead wires. To cut down parasitic e.m.f.'s. the remainder of the circuit (Fig. 5), including the selector switches, is composed entirely of copper. The guard, sample, and cap thermocouples are read with a Leeds and Northrup type K2 potentiometer. Provision is made for simultaneous reversal of the thermocouple, reference junction, and supply, and for a small compensating e.m.f. to neutralize the rather high thermals of the instrument. Two other potentiometers are used, one for heat sink and furnace thermocouples, and the other for the sample top, sample cap, and guard cap thermocouples. A variable e.m.f. is included in the circuit of the centre furnace thermocouple and is used to equalize the e.m.f. from it and the heat sink thermocouple, so that they may be compared without changing the setting of the potentiometer. The resistance thermometer is read with a portable Wheatstone bridge.

*Electrical Shielding*

All possible precautions were taken to eliminate errors arising from electromagnetic effects of other circuits, electrostatic charging, leakage currents or

ceramic conduction at high temperatures. Electromagnetic effects are prevented by using non-inductive windings for all heater elements and by using alternating current only where it is separated from the measuring section

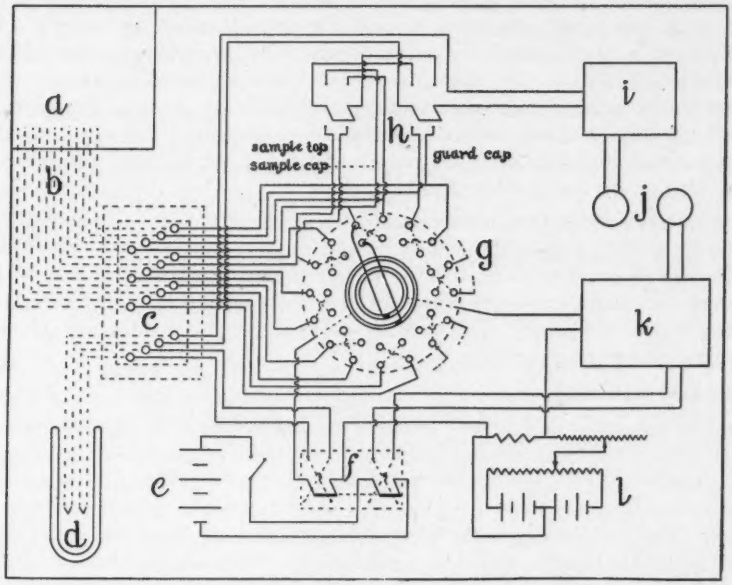



FIG. 5. *Measuring unit thermocouple circuit.*

by the iron pyrostat tube and the iron sleeves inside the furnace. Electrostatic charging arising from low humidity in the winter and from leakage currents due to high humidity in the summer are neutralized by complete shielding of all important leads, by maintaining the apparatus at ground potential, by placing the potentiometers, standard cells, storage batteries, and galvanometers on grounded plates, and by grounding the metal shells of the thermocouple switches and zone box. On the panel all power circuits are kept well separated from the thermocouple circuits. Since the centre column is grounded, and since the thermocouples, connected directly to the column at the tips, are within a few millivolts of ground at all times, there is little possibility of appreciable leakage through the ceramic tubing when readings are being taken. However, the two caps are in the neighborhood of + 20 v. while for shielding purposes it is desirable that their thermocouples be at ground potential. To accomplish this and at the same time neutralize the effect of conduction through the cement in which these thermocouples are embedded, they are grounded at the tips by 0.005 platinum wires that run parallel to the leads as far as the heat sink.

*Thermal Shielding and Lead Losses*

Heat exchange between the sample and sample cap and other parts of the apparatus can be prevented only by complete matching of temperatures. In this apparatus, radiation is the greatest problem, the most vulnerable areas being the top of the sample heater and the upper part of the sample. An isothermal surface is obtained on the heater by a cap of high conductivity material (i.e., gold). Radiation losses are then prevented by means of a second isothermal surface (the inside of the guard cap) at the same temperature. Radiation losses from the sample are prevented by matching the temperature gradients along the sample and the guard sleeves. Heaters are provided on the guard sleeve for this purpose.

Heat losses along the thermocouple leads are kept small by using very fine wire (0.003 in.) and correspondingly small ceramic tubing. Only one other lead need be considered, that to the sample heater, and since it connects the sample and guard caps, which are at the same temperature, heat conduction along it does not occur. The vacuum serves to prevent conduction through the gas, as well as chemical action.

*Assembly of the Apparatus*

After the supporting column and heat sink are installed, the other parts and their associated leads are put in place in the following order. The sample, with heater and cap already attached, is tinned to the heat sink and the sample thermocouples are installed. The guard sleeve is similarly joined to the heat sink. The sample cap thermocouple is threaded through the guard cap, which is then placed on top of the guard sleeve. After the two thermocouples between the guard sleeve and the pyrostat wall are installed, the pyrostat tube is put in place and the furnace is then lowered to a position midway along the pyrostat tube.

*Experimental Procedure*

In order to measure the thermal conductivity it is necessary to adjust the various heater currents in such a way that a steady temperature gradient (2° to 4° C. per cm.) is set up in the sample and that the temperatures of the guard thermocouples are matched to the corresponding ones of the sample. After steady conditions have been maintained for some time, the required quantities may be measured.

It is necessary to regulate the temperature of the heat sink quite accurately if steady conditions are to be maintained in the sample. This is accomplished by means of the heat sink heater in conjunction with the cooling coil. This dual control system enables measurements to be taken over the full temperature range with a single apparatus.

The following sequence of operations was found most satisfactory:

1. The heat sink and furnace are brought to the desired temperatures and maintained constant.
2. The desired gradient is established in the sample.

3. Using the top guard heaters, the temperature of the top guard thermocouple is matched and held to that of the top sample.
4. The guard cap temperature is adjusted until the sample cap thermocouple gives the same reading at equilibrium conditions as the guard cap thermocouple.
5. The furnace and lower guard heater are adjusted until the temperature of the bottom guard thermocouple matches that of the bottom sample.
6. The matching conditions are maintained until the sample comes to thermal equilibrium.
7. Several complete sets of readings are taken. From these results the thermal conductivity is calculated.

*Calculations*

$Q$ as required in Equation (1) is determined from the meter readings by the formula

$$Q = \frac{V}{J}\left(I - \frac{V}{r_1}\right)\left(1 + \frac{r_2}{r_1} - \frac{r_3}{R}\right) \text{ cal. per sec.} \tag{2}$$

where $V$ and $I$ are the voltmeter and ammeter readings, $r_1$ = voltmeter resistance, $r_2$ = resistance of voltmeter leads, $r_3$ = effective resistance of power lead joining the caps, $R$ = heating element resistance, and $J$ = the electrical equivalent of heat. $T_2$ and $T_1$ are the temperatures at the positions of the two thermocouples on the sample, as calculated from the thermocouple e.m.f.'s.

The conductivity was therefore obtained from the formula:

$$K_T = \frac{L_0 V\left(1 - \frac{V}{r_1}\right)\left(1 + \frac{r_2}{r_1} - \frac{r_3}{R}\right)}{A_0 J\,(1 + \alpha\, T)\,(T_2 - T_1)}, \tag{3}$$

where $K_T$ is the average thermal conductivity over the temperature interval $T_2 - T_1$ and is considered to apply to the temperature

$$T = (T_2 + T_1)/2.$$

The parameters $L$ and $A$ in Equation (1) are functions of temperature. For most metals the ratio $\frac{L}{A}$ may be determined with sufficient accuracy from the relation $\frac{L}{A} = \frac{L_0}{A_0\,(1 + \alpha\, T)}$, where $L_0$ and $A_0$ are the dimensions at 0° C. and $\alpha$ = mean linear coefficient of expansion from 0° to 800° C.

*Calibration*

The method used in this experiment of intercalibrating thermocouples could, with modifications, have many other applications, and therefore a full description is included here.

The method is based on the fact that the only information required for a measurement of the thermal conductivity is the magnitude of the change in the temperature gradient brought about by a change in the heat input. It is

not necessary that the initial temperature gradient, heat exchange with surroundings, or power input be zero, nor is it necessary to know the absolute temperature accurately. However, the change in temperature gradient must be the result of the change in the power input alone, and this requires that the exchange between the sample and its surroundings must remain constant.

The procedure in comparing thermocouples is as follows. The furnace and heat sink are brought to the desired temperature and held at this temperature with no power delivery to the sample and guard sleeve heaters. The guard cap temperature is then adjusted until the guard cap and sample cap thermocouples give identical and constant readings. The furnace temperature is then adjusted until the sample top and guard top thermocouples give identical readings. These conditions (constant temperature of heat sink, equality of cap thermocouples, and equality of guard and sample top thermocouples) are held until the e.m.f. difference between the top and bottom sample thermocouples becomes constant. As soon as stable conditions have been reached the differences of e.m.f. between the top and bottom sample thermocouples and the bottom guard and bottom sample thermocouples are measured, using galvanometer deflections to avoid potentiometer errors. It has been found that intercalibration at 60° to 100° C. intervals is usually sufficient.

During a measurement, conditions are arranged so that the heat exchange from any small area of surface of the sample is the same as it was during the intercalibration. This is accomplished by matching the readings of the guard cap and sample cap, the guard top and sample top, and the guard bottom and sample bottom thermocouples, respectively, in the last case making due allowance for the calibration differences. Thus the change in the temperature gradient along the sample is due to the measured heat input alone. In the calculations the necessary correction is applied to the bottom sample thermocouple reading.

*Experimental Error*

The following are possible sources of error in this apparatus:

1. Heat loss from the sample and sample cap by radiation.
2. Heat loss by conduction along power leads, thermocouple leads, and ceramic tubing.
3. Non-linearity of heat flow in the sample.
4. Errors in measurement of power input.
5. Errors in measurement of the temperature interval.
6. Errors due to the apparatus not being at equilibrium.
7. Errors in measurement of dimensions.
8. Errors arising from the variation of conductivity with temperature.

1. The methods used to reduce the heat loss from the sample by radiation were discussed previously. Matching between thermocouples during a run was maintained to better than 0.1° C. Taking the entire effective radiation area into consideration and using Stefan's law of radiation with an assumed

effective emissivity of 0.6 between close surfaces, the total loss at 1000° A from radiation amounts to less than 0.30% of the heat input, and decreases as the cube of the absolute temperature.

2. Total conduction of heat along the 0.003 in. thermocouple leads and 2 mm. ceramic tubing with the maximum gradient of 4° C. per cm. and along the 0.010 in. lead wire with a gradient of less than 0.03° C. per cm. could not possibly cause an error greater than 0.05%.

3. Non-linearity of heat flow in the sample would be caused primarily by poor thermal contact between the sample heater and the sample, or between the sample and the heat sink, and to a lesser extent by radiation from the surface. As tin is used at the interfaces, large discontinuities are prevented. In addition, the measuring thermocouples are spaced 1 cm. and 2 cm. from the top and bottom surfaces, respectively, a distance that should be sufficient to allow the local disturbances to level out. Radiation losses from the surface of the sample are kept small by the shielding sleeve, and it can be shown that the effect of radiation on linearity would introduce a maximum error of less than 0.05%.

4. Errors in measurement of power input could arise from the resistance of the voltmeter lead, loss of heat generated in the lead between the two caps, power losses between the sample heater and the ground connection, and limitations of accuracy of meter readings. The voltmeter lead resistance is allowed for in Equation (3) for $K_T$. Power generated in the lead between the caps is 0.7% of the total and for purposes of Equation (1) it is assumed that approximately 0.4% is lost to the guard cap. The net correction applied by these terms in the equation is 0.25% with an uncertainty in the order of 0.20%. Power losses from the heater to ground have been measured using the top sample thermocouple as potential lead, and are negligible. By setting one meter on a scale graduation, by careful calibration, and by using only the top part of the scales, the error due to meter readings may be kept below 0.25%.

5. Errors in the measurement of the temperature interval can arise from thermocouple calibration, potentiometer readings, parasitic e.m.f.'s in the potentiometer and circuits, or lead conduction. On account of the method of intercalibration of thermocouples it is unnecessary to calibrate accurately with respect to the international temperature scale. An error in this respect creates corresponding errors in the calculated temperature interval and in the temperature to which the determination is applied. For a substance whose conductivity decreases with increasing temperature (e.g., most pure metals) these two errors tend to cancel each other, and the net effect would not be more than 0.1% under any reasonable conditions. It should be noted here that the sample top, sample cap, and guard cap thermocouples provide a useful check on one another since an error in e.m.f. of any one of the three would make it impossible to match them when calibrating. In the measurements on Armco iron, the difference in reading between any two never exceeded 2 $\mu$v. at the highest temperatures, and therefore it seems unlikely that any

effective contamination occurred. The relative calibration of the sample thermocouples was reproducible at all temperatures to less than 0.2 $\mu$v., which represents a possible error of less than 0.2%. Because of the compensating e.m.f. and the provision for reversal in the potentiometer circuit, it is possible to reproduce readings to the full sensitivity of the potentiometer (approximately 0.05% of the interval). The slide-wire of the potentiometer has been checked and the error does not exceed 0.1%. Since both thermocouples were carried around the sample for a distance of 4 cm. in a constant temperature area and the subsequent gradient was less than 4° C. per cm., and since both are subjected to identical conditions, the errors in reading due to lead conduction should be negligible and certainly would not be more than 0.05%. The total of these errors is less than 0.5%.

6. At higher temperatures the time required to reach equilibrium is greater on account of the lower conductivity and greater heat capacity of the sample. In order to be certain that conditions are in equilibrium at the time of measurement, readings were not accepted until three successive sets showed no appreciable drift. Using accepted values for the specific heat of iron, gold, and ceramic cement, it can be shown that for an iron sample a drift of 1/100° C. per min. corresponds to a heat absorption or emission of approximately 1/60 w., or 0.1% of the power input. No readings were accepted where over a period of 15 min. there was an average drift of more than 1/200° C. per min.

7. The diameter of the sample is measured at room temperatures to an accuracy of 0.1%, and the separation of the thermocouples is measured by means of a travelling microscope to approximately 0.2%. After correction for thermal expansion of the sample the total error in dimensions would not exceed 0.4%. This error does not affect relative readings.

8. For substances with a linear conductivity–temperature relation, use of a large temperature interval introduces no error in the conductivity, as calculated from Equation (3). However, if the relation is non-linear, an error is introduced which varies as the square of the temperature interval. The advantage of being able to make accurate measurements using a small interval is obvious. The apparatus herein described can be used with temperature intervals as small as 5° C.

Effects due to work hardening on the surfaces of the sample are negligible under ordinary conditions. In any event the past history of the specimen does not influence the accuracy of any one thermal conductivity measurement. However, changes caused by annealing would affect the consistency with which results could be reproduced, and should immediately become evident.

The sum of errors from all sources is 1.95%. Of this, 0.90% is systematic and 0.95% random error. The estimate of random error is well verified by the results of measurements on Armco iron. In this case the maximum deviation from the average curve is 0.6% and the standard deviation 0.35%.

## Measurements on Armco Iron

*Introduction*

Armco ingot iron was selected as the test metal for several reasons. It may be readily obtained in a state of reasonable purity. Therefore the results of previous determinations (2, 3) could serve as a check on the accuracy of the apparatus. The thermal conductivity shows no sharp anomalies in the range 0° to 800° C. and is reasonably close to that of many of the materials that will later be tested. Aside from oxidation, iron is not subject to appreciable change of properties as a result of heating and should give reproducible results if a sufficiently high vacuum is maintained.

*The Sample*

The sample was a solid cylinder 2.50 cm. in diameter and 8.00 cm. in length, machined from a hot rolled 1½ in. rod. Chemical analysis gave the following composition:

| | |
|---|---|
| Copper | 0.067% |
| Manganese | 0.035 |
| Nickel | 0.024 |
| Sulphur | 0.039 |
| Carbon | 0.028 |
| Iron (by difference) | 99.808 |

*Results and Discussion*

The results are tabulated in the Appendix in the order in which the measurements were taken. In Fig. 6 the thermal conductivity is plotted against temperature for the range 0° to 730° C. with extrapolation to 800° C. Readings were not taken above 730° C. because a thermocouple broke in a place that would require partial dismantling of the apparatus. As measurements on Armco iron were made chiefly to test the reliability of the apparatus it was not felt necessary to reassemble it for further readings at high temperatures.

From the experimental results, values have been determined at 100° intervals from 0° to 800° C., and these values are shown in Table I. Included in the table are values obtained by Powell (2) and van Dusen and Shelton (3) for iron of comparable purity.

The results of this determination agree well with those of Powell but are higher than those of van Dusen and Shelton at low temperatures. From the plotted results of the latter it would appear as if a curve with larger slope at low temperatures would have fitted the experimental points as well as the straight line that was used, and would have brought the average values closer to those of the other determinations. However, none of the differences are greater than those that might be expected from experimental error and variations in the samples.

It will be noted in Fig. 6 that a change of slope in the curve of conductivity against temperature occurs at about 375° C., while the sections of the curve above and below this point are relatively linear. Straight lines have been fitted to the experimental points by the method of least squares, giving

$K = 0.1819 - 1.631 \times 10^{-4} T$ below 375° C. and $K = 0.1656 - 1.197 \times 10^{-4} T$ from 375° to 800° C. The two lines intersect at $T = 377°$ C. The deviations of the experimental points from these lines have been plotted in

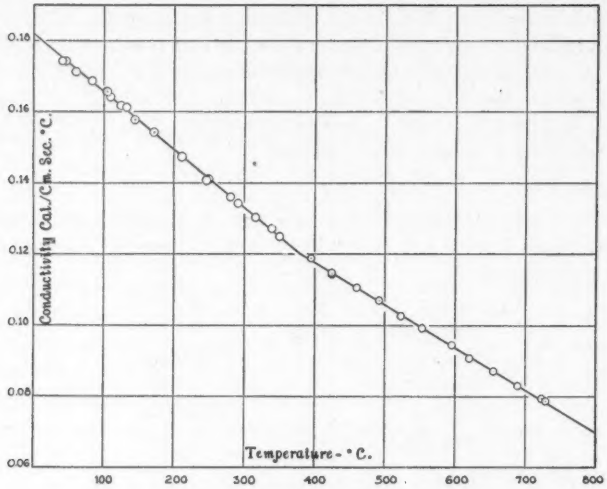



FIG. 6. *Thermal conductivity of Armco iron.*

TABLE I

THERMAL CONDUCTIVITY OF ARMCO IRON

| Temperature, ° C. | Thermal conductivity, c.g.s. units | | |
|---|---|---|---|
| | Armstrong and Dauphinee | Powell | van Dusen and Shelton |
| 0 | $0.181_9$ | 0.177 | 0.172 (estimate) |
| 100 | $0.165_6$ | 0.163 | 0.159 |
| 200 | $0.149_3$ | 0.147 | 0.145 |
| 300 | $0.133_0$ | 0.132 | 0.131 |
| 400 | $0.117_7$ | 0.116 | 0.1175 |
| 500 | $0.105_7$ | 0.1035 | 0.104 |
| 600 | $0.093_7$ | 0.093 | — |
| 700 | $0.081_7$ | 0.082 | — |
| 800 | $0.069_8$ | 0.071 | — |

Fig. 7, with differences from the first line being shown over the full range 0° to 800° C. in order to amplify the change in slope. The maximum deviation from the calculated lines is 0.6% and the standard deviation is 0.35%. It is thought that the change of slope in the conductivity–temperature curve may be due to the effect of the nickel impurity in the sample, the intersection of the two lines falling almost exactly at the Curie point of nickel (376° C.).

However, the magnitude of the effect (a change in slope of 25%) is rather large for the amount of impurity present (0.024%). It should be noted that Powell's results show a bend in the curve in the neighborhood of 405° C. but

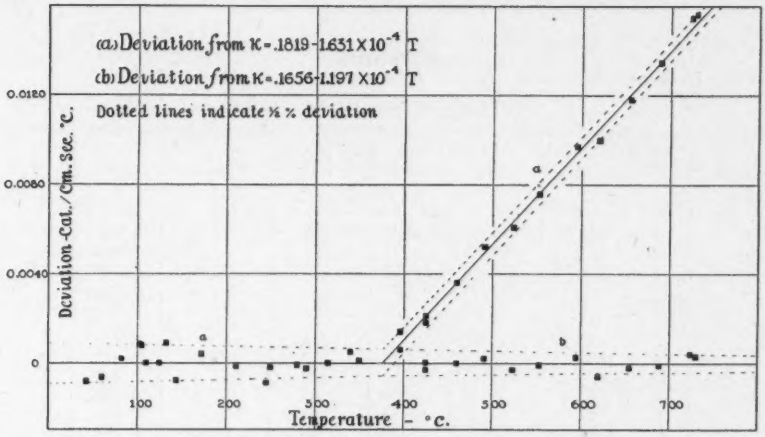



FIG. 7. *Deviation from calculated curves.*

the analysis of his sample showed no detectable nickel impurity. However, Powell's sample was nickel-plated, and the bend in his curve might be explained by either thermal diffusion or by error in the values for the conductivity of nickel used in the corrections. Further conclusions are not justified at present. Proposed work on the electrical and thermal conductivities of this sample and others of higher purity should indicate more definitely the reason for such an anomaly.

## Conclusions

An apparatus has been described for accurate measurement of thermal conductivities of metals in vacuum for the temperature range 0° to 800° C. Measurements on a sample of Armco iron indicate that absolute error in measurements is not more than 2% and the relative error considerably less than 1%. The results on the iron sample agree well with those of other determinations on iron of comparable purity.

## Acknowledgments

In conclusion the authors wish to acknowledge their indebtedness to Dr. J. D. Babbitt for his interest and constructive criticism at all stages of the work, and to Mr. C. St. Jacques, Mr. P. Huot, and Mr. J. MacDonald for excellent co-operation and technical skill in the construction and assembly of the apparatus, and in the wiring of the control circuits.

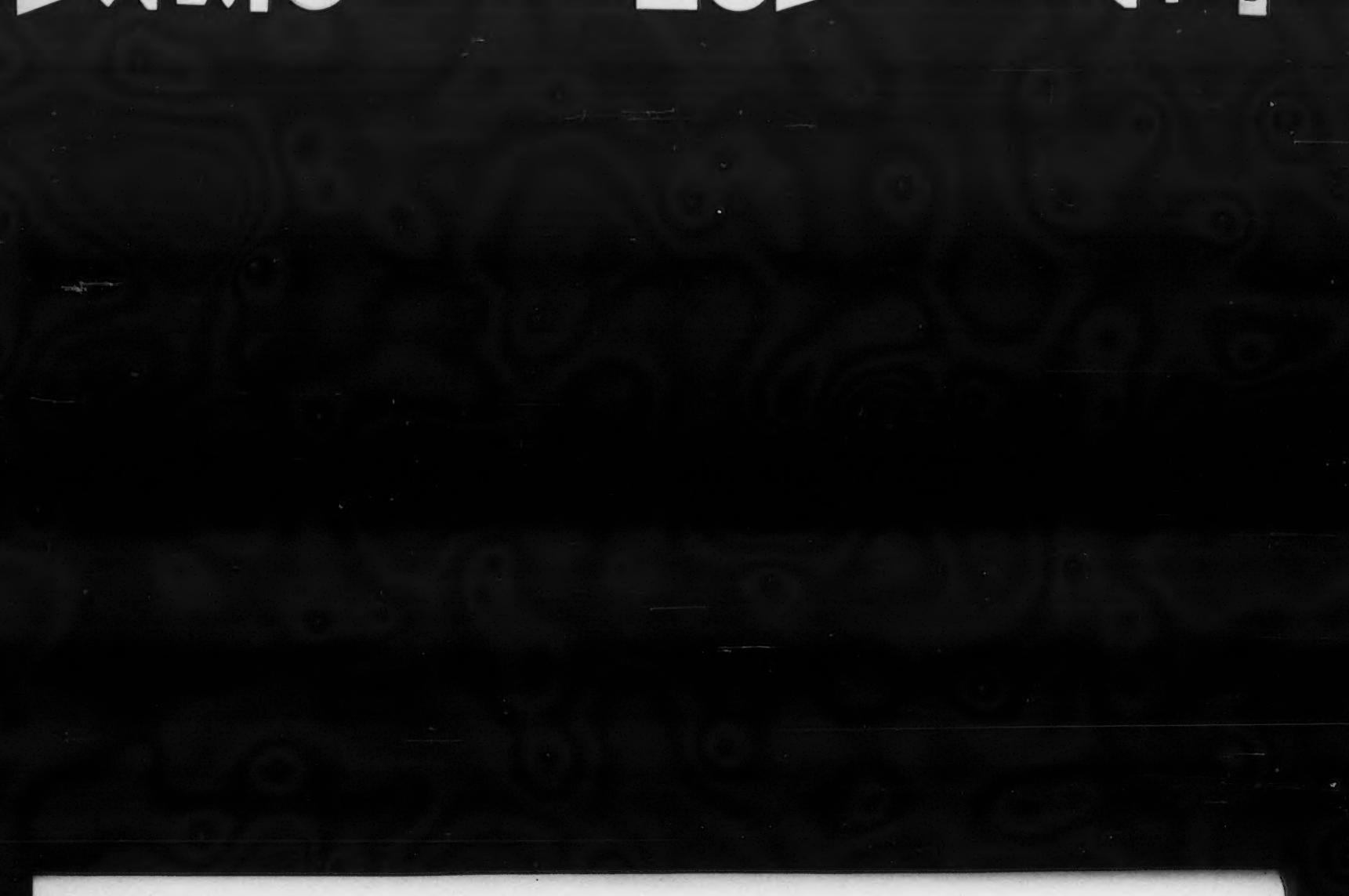
## References

1. ARMSTRONG, L. D. and DAUPHINEE, T. M. Can. J. Research, F, 25 : 221-225. 1947.
2. POWELL, R. W. Proc. Phys. Soc., London, 46 : 659-674. 1934.
3. VAN DUSEN, M. S., and SHELTON, S. M. Bur. Standards J. Research, 12 : 429-440. 1934.

## APPENDIX

THERMAL CONDUCTIVITY OF METALS

| Date | Run No. | $T_2$ | $T_1$ | $T_2 - T_1$ | $T = \frac{T_2+T_1}{2}$ | $V$, corr. | $I$, corr. | $K_t$ |
|---|---|---|---|---|---|---|---|---|
| Jan. 8 | 1 | 108.77 | 99.54 | 9.23 | 104.1 | 14.16 | 0.444 | 0.1658 |
| | 2 | 112.28 | 98.07 | 14.21 | 105.2 | 17.78 | 0.543 | 0.1656 |
| Jan. 9 | 3 | 177.05 | 166.40 | 10.65 | 171.7 | 15.38 | 0.439 | 0.1543 |
| | 4 | 137.79 | 127.61 | 10.18 | 132.7 | 14.98 | 0.450 | 0.1612 |
| | 5 | 218.09 | 204.59 | 13.50 | 211.4 | 17.44 | 0.469 | 0.1473 |
| Jan. 10 | 6 | 253.59 | 239.70 | 13.89 | 246.7 | 17.65 | 0.456 | 0.1408 |
| | 7 | 287.20 | 273.53 | 13.67 | 280.3 | 17.48 | 0.438 | 0.1361 |
| | 8 | 323.27 | 307.91 | 15.36 | 315.6 | 18.53 | 0.445 | 0.1304 |
| Jan. 11 | 9 | 46.28 | 38.23 | 8.06 | 42.2 | 12.92 | 0.446 | 0.1742 |
| | 10 | 67.66 | $54.77_8$ | $12.88_8$ | 61.2 | 16.64 | 0.544 | 0.1713 |
| | 11 | $89.77_8$ | 76.29 | $13.48_8$ | 83.0 | 17.19 | 0.543 | 0.1686 |
| Jan. 13 | 12 | 358.27 | 341.92 | 16.35 | 350.1 | 18.99 | 0.443 | 0.1249 |
| | 13 | 403.20 | 385.35 | 17.85 | 395.3 | 19.77 | 0.442 | 0.1188 |
| | 14 | 433.25 | 416.53 | 16.71 | 424.8 | 18.97 | 0.417 | 0.1147 |
| | 15 | 470.11 | 449.74 | 20.37 | 459.6 | 20.88 | 0.445 | 0.1105 |
| | 16 | 502.81 | 481.29 | 21.52 | 491.9 | 21.35 | 0.445 | 0.1069 |
| | 17 | 535.48 | 512.53 | 22.95 | 523.0 | 21.87 | 0.445 | 0.1026 |
| | 18 | 563.89 | 542.33 | 21.56 | 553.1 | 21.04 | 0.420 | 0.0992 |
| Jan. 15 | 19 | 433.66 | 416.85 | 16.81 | 424.7 | 18.97 | 0.418 | 0.1144 |
| | 20 | 347.23 | 331.06 | 16.17 | 339.1 | 18.96 | 0.447 | 0.1272 |
| | 21 | 257.69 | 241.06 | 16.63 | 249.3 | 19.41 | 0.497 | 0.1411 |
| Jan. 16 | 22 | 607.15 | 583.93 | 23.22 | 595.5 | 21.61 | 0.420 | 0.0945 |
| | 23 | 631.43 | 609.70 | 21.73 | 620.5 | 20.64 | 0.395 | 0.0907 |
| | 24 | 666.04 | 642.78 | 23.26 | 654.3 | 21.21 | 0.395 | 0.0870 |
| | 25 | 700.72 | 676.85 | 23.87 | 688.7 | 21.23 | 0.386 | 0.0830 |
| | 26 | 736.35 | 711.18 | 25.17 | 723.7 | 21.56 | 0.384 | 0.0793 |
| | 27 | 742.33 | 715.33 | 27.00 | 728.8 | 22.29 | 0.395 | 0.0786 |
| Jan. 20 | 28 | 132.38 | 117.30 | 15.08 | 124.7 | 18.43 | 0.543 | 0.1616 |
| | 29 | 116.89 | 103.00 | 13.89 | 109.9 | 17.58 | 0.532 | 0.1640 |
| | 30 | 151.14 | 136.74 | 14.40 | 143.9 | 17.98 | 0.519 | 0.1577 |
| Jan. 24 | 31 | 298.32 | 284.09 | 14.23 | 291.1 | 17.94 | 0.438 | 0.1342 |



# CANADIAN JOURNAL OF RESEARCH

## Notes on the Preparation of Copy

GENERAL:—Manuscripts should be typewritten, double spaced, and the **original and at least one extra copy** submitted. Style, arrangement, spelling, and abbreviations should conform to the usage of this Journal. Names of all simple compounds, rather than their formulae, should be used in the text. Greek letters or unusual signs should be written plainly or explained by marginal notes. Superscripts and subscripts must be legible and carefully placed. Manuscripts should be carefully checked before being submitted, to reduce the need for changes after the type has been set. **All pages, whether text, figures, or tables, should be numbered.**

ABSTRACT:—**An abstract of not more than about 200 words, indicating the scope of the work and the principal findings, is required.**

ILLUSTRATIONS:

(i) *Line Drawings:*—All lines should be of sufficient thickness to reproduce well. Drawings should be carefully made with India ink on white drawing paper, blue tracing linen, or co-ordinate paper **ruled in blue only**; any co-ordinate lines that are to appear in the reproduction should be ruled in black ink. Paper ruled in **green, yellow, or red should not be used** unless it is desired to have all the co-ordinate lines show. Lettering and numerals should be neatly done in India ink preferably with a stencil (**do not use typewriting**) and be of such size that they will be legible and not less than one millimetre in height when reproduced in a cut three inches wide. All experimental points should be carefully drawn with instruments. Illustrations need not be more than two or three times the size of the desired reproduction, but the ratio of height to width should conform with that of the type page. **The original drawings and one set of small but clear photographic copies are to be submitted.**

(ii) *Photographs:*—Prints should be made on glossy paper, with strong contrasts; they should be trimmed to remove all extraneous material so that essential features only are shown. Photographs should be submitted **in duplicate**; if they are to be reproduced in groups, one set should be so arranged and mounted on cardboard with rubber cement; the duplicate set should be unmounted.

(iii) *General:*—**The author's name, title of paper, and figure number should be written on the back of each illustration.** Captions should not be written on the illustrations, but typed on a separate page of the manuscript. All figures (including each figure of the plates) should be numbered consecutively from 1 up (arabic numerals). **Each figure should be referred to in the text.**

TABLES:—Titles should be given for all tables, which should be numbered in Roman numerals. Column heads should be brief and textual matter in tables confined to a minimum. **Each table should be referred to in the text.**

REFERENCES:—**These should be listed alphabetically by authors' names, numbered in that order, and placed at the end of the paper.** The form of literature citation should be that used in this Journal. **Titles of papers should not be given in references listed in Sections A, B, E, and F, but must be given in references listed in Sections C and D. All citations should be checked with the original articles.** Each citation should be referred to in the text by means of the key number; in Sections C and D the author's name and the date of publication may be included with the key number if desired.

The *Canadian Journal of Research* conforms in general with the practice outlined in the *Canadian Government Editorial Style Manual*, published by the Department of Public Printing and Stationery, Ottawa.

## Reprints

Fifty reprints of each paper are supplied free. Additional reprints, if required, will be supplied according to a prescribed schedule of charges.

